CHALMERS

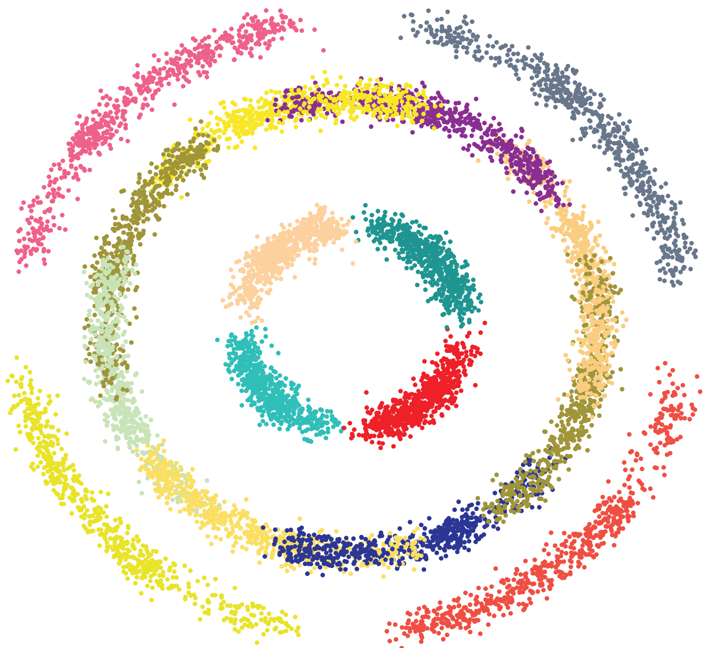

Modeling and Estimation of Phase Noise in Oscillators with Colored Noise Sources

M. Reza Khanzadi

Communication Systems Group
Department of Signals and Systems

Microwave Electronic Laboratory
Department of Microtechnology and Nanoscience

CHALMERS UNIVERSITY OF TECHNOLOGY
Göteborg, Sweden

THESIS FOR DEGREE OF LICENTIATE OF ENGINEERING

Modeling and Estimation of Phase Noise in Oscillators with Colored Noise Sources

M. Reza Khanzadi

CHALMERS

Communication Systems Group
Department of Signals and Systems

Microwave Electronic Laboratory
Department of Microtechnology and Nanoscience

Chalmers University of Technology

Göteborg, August 2013

Khanzadi, M. Reza
Modeling and Estimation of Phase Noise in Oscillators with Colored Noise Sources

Technical Report No. R019/2013
ISSN 1403-266X

Communication Systems Group
Department of Signals and Systems
Chalmers University of Technology
SE-412 96 Göteborg, Sweden
Telephone: + 46 (0)31-772 1000

Microwave Electronic Laboratory
Department of Microtechnology and Nanoscience
Chalmers University of Technology
SE-412 96 Göteborg, Sweden
Telephone: + 46 (0)31-772 1000

Homepage: http://khanzadi.info
Email: khanzadi@chalmers.se

This thesis has been prepared using LaTeX.

Front Cover: The figure on the front cover is the distorted received signal constellation of a 16-QAM communication system due to transmitter and receiver oscillator phase noise.

Printed by Chalmers Reproservice,
Göteborg, Sweden, August 2013.

To my beloved Fatemeh

ABSTRACT

The continuous increase in demand for higher data rates due to applications with massive number of users motivates the design of faster and more spectrum efficient communication systems. In theory, the current communication systems must be able to operate close to Shannon capacity bounds. However, the real systems perform below capacity limits, mainly due to channel estimation error and hardware impairments that have been neglected by idealistic or simplistic assumptions on the imperfections.

Oscillator phase noise is one of the hardware impairments that is becoming a limiting factor in high data rate digital communication systems. Phase noise severely limits the performance of systems that employ dense constellations. Moreover, the level of phase noise (at a given off-set frequency) increases with carrier frequency which means that the problem of phase noise may be even more severe in systems with high carrier frequency.

The focus of this thesis is on finding accurate statistical models of phase noise, as well as the design of efficient algorithms to mitigate the effect of this phenomenon on the performance of modern communication systems. First we derive the statistics of phase noise with white and colored noise sources in free-running and phase-locked-loop-stabilized oscillators. We investigate the relation between real oscillator phase noise measurements and the performance of communication systems by means of the proposed model. Our findings can be used by hardware and frequency generator designers to better understand the effect of phase noise with different sources on the system performance and optimize their design criteria respectively.

Then, we study the design of algorithms for estimation of phase noise with colored noise sources. A soft-input maximum a posteriori phase noise estimator and a modified soft-input extended Kalman smoother are proposed. The performance of the proposed algorithms is compared against that of those studied in the literature, in terms of mean square error of phase noise estimation, and symbol error rate of the considered communication system. The comparisons show that considerable performance gains can be achieved by designing estimators that employ correct knowledge of the phase noise statistics. The performance improvement is more significant in low-SNR or low-pilot density scenarios.

Keywords: Oscillator Phase Noise, Voltage-controlled Oscillator, Phase-Locked Loop, Colored Phase Noise, Phase Noise Model, Bayesian Cramér-Rao Bound, Maximum a Posteriori Estimator, Extended Kalman Filter/Smoother, Mean Square Error.

LIST OF PUBLICATIONS

Appended papers

Paper A
M. Reza Khanzadi, Dan Kuylenstierna, Ashkan Panahi, Thomas Eriksson, and Herbert Zirath, "Calculation of the Performance of Communication Systems from Measured Oscillator Phase Noise," *Accepted for publication in IEEE Transactions on Circuits and Systems I,* Aug. 2013.

Paper B
M. Reza Khanzadi, Rajet Krishnan, and Thomas Eriksson, "Estimation of Phase Noise in Oscillators with Colored Noise Sources," *Accepted for publication in IEEE Communications Letters,* Aug. 2013.

Other publications

[J1] Rajet Krishnan, **M. Reza Khanzadi**, Thomas Eriksson, and Tommy Svensson, "Soft metrics and their Performance Analysis for Optimal Data Detection in the Presence of Strong Oscillator Phase Noise," *IEEE Transactions on Communications,* Jun. 2013.

[J2] Hani Mehrpouyan, **M. Reza Khanzadi**, Michail Matthaiou, Robert Schober, and Yingbo Hua, "Improving Bandwidth Efficiency in E-band Communication Systems," *Submitted to IEEE Communications Magazine,* Sep. 2012.

[C1] **M. Reza Khanzadi**, Rajet Krishnan, and Thomas Eriksson,"Effect of Synchronizing Coordinated Base Stations on Phase Noise Estimation," *IEEE Conference on Acoustic, Speech, and Signal Processing (ICASSP),* May. 2013.

[C2] **M. Reza Khanzadi**, Ashkan Panahi, Dan Kuylenstierna, and Thomas Eriksson, "A model-based analysis of phase jitter in RF oscillators," *IEEE International Frequency Control Symposium (IFCS),* May. 2012.

[C3] Rajet Krishnan, **M. Reza Khanzadi**, Lennart Svensson, Thomas Eriksson, and Tommy Svensson, "Variational Bayesian Framework for Receiver Design in the Presence of Phase Noise in MIMO Systems," *IEEE Wireless Communications and Networking Conference (WCNC),* Apr. 2012.

[C4] **M. Reza Khanzadi**, Hani Mehrpouyan, Erik Alpman, Tommy Svensson, Dan Kuylenstierna, and Thomas Eriksson,"On models, bounds, and estimation algorithms for time-varying phase noise,"*IEEE International Conference on Signal Processing and Communication Systems (ICSPCS),* Dec. 2012.

[C5] **M. Reza Khanzadi**, Kasra Haghighi, and Thomas Eriksson, "Optimal Modulation for Cognitive Transmission over AWGN and Fading Channels,"*IEEE European Wireless Conference,* Apr. 2011.

[C6] **M. Reza Khanzadi**, Kasra Haghighi, Ashkan Panahi, and Thomas Eriksson, "A Novel Cognitive Modulation Method Considering the Performance of Primary User," *IEEE Wireless Advanced Conference (WiAD)* Jun. 2010.

[C7] Arash Toyserkani, **M. Reza Khanzadi**, Erik Ström, and Arne Svensson, "A Complexity Adjustable Scheduling Algorithm for Throughput Maximization in Clusterized TDMA Networks,"*IEEE Vehicular Technology Conference (VTC),* May. 2010.

ACKNOWLEDGEMENTS

Doing a *PhD* is a journey to the unknown! You do not know where to start and your destination may not be clearly known either! On such a journey the last thing you need is to be alone. It is always the support and help of the people around you, which makes you feel **P**assionate, **h**opeful, and **D**eveloping on this journey.

Now in the middle of this journey I would like to express my deepest gratitude to my supervisor Prof. Thomas Eriksson who has always supported me with his sharp insight and invaluable feedback. Thomas, you have always been my best source of motivation. My greatest gratitude also goes to my examiner Prof. Herbert Zirath for his generous support. I hope I can learn more and more from you during the rest of my PhD. I would also like to offer my special thanks to my co-supervisor and my sport hero Dr. Dan Kuylenstierna for all his constructive comments and warm encouragement. I really enjoy our discussions and look forward to more of those and further possibilities of learning from you. My appreciation also goes to Prof. Erik Ström for giving me the opportunity to be a part of ComSys family.

Special thanks to Rajet Krishnan, my research buddy and a great officemate, for all fruitful discussions we have. As experience has shown the Thomas-Reza-Rajet triangle rocks in writing papers! Let's keep it up! I also need to thank Dr. Hani Mehrpouyan, who made me more interested in estimation theory and for all his support during his stay in Sweden. And finally my friend Ashkan Panahi, I learned from you how to tackle a problem. Thanks for all intensive discussions inside and outside the university.

Former and current colleagues at S2 and MC2, and my friends

Neda Tilak Fredrik Nima Arezoo Mitra Ashkan Behrooz Ali Astrid Ahmed Amirsepehr Christopher Fatemeh Hamidreza Abu Arash Erik Gabbo Christian Abouzar Cristian Elena Lars Hani Guillermo Johnny Hojjat Giuseppe Jessica Keerthi Jingya Henk Aidin Natasha Katharina Lotfollah Kasra Livia Negar Maryam Michalis Madeleine Lai Soodabeh Mohammadreza Tommy Roozbeh Sahar Srikar Wanlu Agneta Misha Rajet Naga Wei Sima Toktam Jenny Mona Yutao Ulf Alex Mehdi Sonia Lennart Rocco

thank you for being there and supporting me.

My sincerest gratitude goes to my family and their never-ending support. Shirin, Shohreh, and Giti, thank you for everything.

Last but not least, my beloved Fatemeh, you have always been there for me in all the tears and laughs of this PhD life! Thank you for your love, support and patience. You are the only one from *management* world who knows a lot about *oscillator phase noise* now!

M. Reza Khanzadi
Göteborg August 2013

CONTENTS

ACRONYMS

ADC: Analog to Digital Converter

AR: Autoregressive

AWGN: Additive White Gaussian Noise

BCRB: Bayesian Cramér-Rao Bound

BER: Bit Error Rate

BIM: Bayesian Information Matrix

CRB: Cramér-Rao Bound

EKS: Extended Kalman Smoother

EVM: Error-Vector Magnitude

FIM: Fisher Information Matrix

GaN: Gallium Nitride

HEMT: High-Electron-Mobility Transistor

I/Q: Inphase / Quadrature Phase

LNA: Low-Noise Amplifier

MAP: Maximum a Posteriori

MBCRB: Modified Bayesian Cramér-Rao Bound

MIMO: Multiple-Input Multiple-Output

ML: Maximum Likelihood

MMIC: Monolithic Microwave Integrated Circuit

MMSE: Minimum Mean Square Error

MSE: Mean Squared Error

OFDM: Orthogonal Frequency Division Multiplexing

PA:	Power Amplifier
PDF:	Probability Density Function
PLL:	Phase-Locked Loop
PN:	Phase Noise
PSD:	Power Spectral Density
QAM:	Quadrature Amplitude Modulation
RF:	Radio Frequency
SER:	Symbol Error Rate
SNR:	Signal-to-Noise Ratio
SSB:	Single-Side-Band

Part I

Introduction

CHAPTER 1

OVERVIEW

1 Introduction

Digital communication has become an indispensable part of our personal and professional lives. Data transmission rates over fixed and wireless networks have been increasing rapidly due to applications with massive number of users such as smartphones, tablets, wired and wireless broadband Internet connections, cloud computing, the machine-to-machine communication services, etc. Demands for higher data rates continue to increase at about 60% per year [1].

This increasing demand motivates the need for design of faster and more spectrum efficient communication systems. Despite the progress in theoretical aspects of such systems, the analog front end still fails to deliver what is promised mainly due shortcomings such as hardware impairments. Hardware impairments in radio-frequency and optical communications, such as amplifier nonlinearity, IQ imbalance, optical channel nonlinearities, and oscillator or laser phase noise, can be seen as the bottlenecks of the performance [2].

A promising solution to overcome this problem is to mitigate the effects of hardware impairments by means of digital signal processing algorithms. A key step in this avenue is to find mathematical models that can accurately represent the physical impairments. In many prior studies, simple models have been employed for this purpose. For instance, using the additive white Gaussian noise has been a normal practice to summarize all unwanted effects from communication channel and hardware components on the transmitted signal. However, to be able to come up with efficient algorithms, better understanding and modeling of the hardware impairments is needed.

Oscillator phase noise (PN) is one of the hardware imperfections that is becoming a limiting factor in high data rate digital communication systems. PN severely limits the performance of systems that employ dense constellations. The negative effect of phase noise is more pronounced in high carrier frequency systems, e.g., E-band (60-80 GHz), mainly due to the high level of PN in oscillators designed for such frequencies [3–5]. Moreover, PN severely affects the performance of multiple antenna (MIMO) systems [6,7], and also destroys the orthogonality of the subcarriers in orthogonal frequency division multiplexing (OFDM) systems that degrades the performance by producing intercarrier interference [8, 9].

In many prior studies, PN is modeled as a discrete random walk with uncorrelated (white) Gaussian increments between each time instant (i.e., the discrete Wiener process). This model results from using oscillators with white noise sources [10]. However, numerous studies show that real oscillators also contain colored noise sources [10–15].

In summary, accurate PN models and efficient algorithms to mitigate the effect of this phenomenon are central to the design of modern communication systems. These aspects form the core of this thesis.

2 Aim of the Thesis

In this thesis, we focus on three important aspects of dealing with PN in communication systems:

- We provide an accurate statistical model for PN in practical oscillators. This model can further be used for accurate simulations of PN-affected communication systems, as well as design of algorithms for compensation of PN.
- We calculate the performance of a PN-affected communication system from given oscillator's PN measurements. Such results can have important effects on design of hardware for frequency generation.
- We design and implement PN estimation algorithms by employing our proposed statistical model. We show that considerable performance improvements can be achieved by using the proposed algorithms, especially in low signal-to-noise ratio (SNR) and low-pilot-density scenarios.

3 Thesis Outline

We start the Chapter 2 of this thesis by explaining different sources of hardware impairments in practical communication systems. Then we focus on PN and describe its effects by introducing a mathematical model for a PN-affected communication system. In Chapter 3, we talk about oscillators, their roles in communication systems, and the sources of PN in oscillators. Further, we propose a new statistical model for the PN of real oscillators. In Chapter 5, we focus on design of algorithms for PN compensation. We describe the basics of Bayesian estimation theory and finish the chapter by describing the bounds on the performance of such estimators. Finally, we summarize our contributions in Chapter 6.

CHAPTER 2

COMMUNICATION SYSTEM MODEL

1 Practical Communication Systems

Hardware impairments are an inevitable consequence of using non-ideal components in communication systems. Any practical communication system consists of several components that play a specific role in the transmission of data stream from one point to another. Fig. 2.1 illustrates a simplified hardware block diagram of a typical wireless communication system.

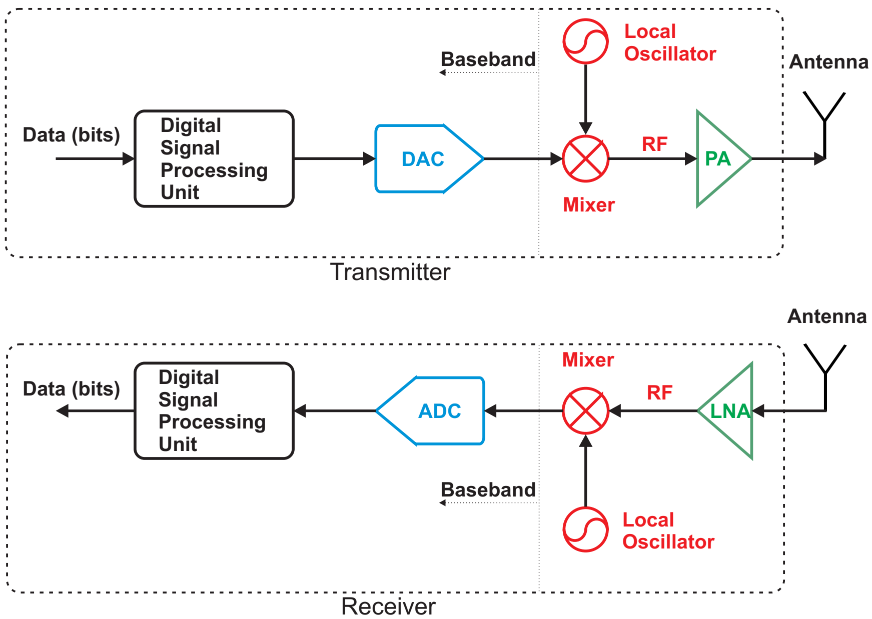

Figure 2.1: Hardware block diagram of the transmitter and receiver in a typical communication system.

All the system components are made of electronic devices such as resistors, inductors, capacitors, diodes, and transistors, which are composed of conductor and semiconductor materials. These electronic devices are not perfect and can behave differently from what is predicted for many reasons such as temperature variation, aging, pressure, etc.

One of the major hardware impairments affecting the performance of communication systems is *oscillator PN*. Oscillators are one of the main building blocks in a communication system. Their role is to create stable reference signals for frequency and timing synchronization. Unfortunately, any real oscillator suffers from hardware imperfections that introduce PN to the communication system. The fundamental source of the PN is the inherent noise of the passive and active components (e.g., thermal noise) inside the oscillator circuitry [11, 16].

2 Model of the Received Signal

Consider a single-carrier single-antenna communication system. The transmitted signal $x(t)$ is

$$x(t) = \sum_{n=1}^{N} s[n]p(t - nT), \tag{2.1}$$

where $s[n]$ denotes the modulated symbol from constellation $\mathcal{C}$ with an average symbol energy of E_s, n is the transmitted symbol index, $p(t)$ is a bandlimited square-root Nyquist shaping pulse function with unit-energy, and T is the symbol duration [17]. The continuous-time complex-valued baseband received signal after down-conversion, affected by the transmitter and receiver oscillator PN, can be written as

$$r(t) = x(t)e^{j\phi(t)} + \tilde{w}(t), \tag{2.2}$$

where $\phi(t)$ denotes the PN process and $\tilde{w}(t)$ is zero-mean circularly symmetric complex-valued additive white Gaussian noise (AWGN), that models the effect of noise from other components of the system. The received signal (2.2) is passed through a matched filter $p^*(-t)$ and the output is

$$\begin{aligned} y(t) = &\int_{-\infty}^{\infty} \sum_{n=1}^{N} s[n]p(t - nT - \tau)p^*(-\tau)e^{j\phi(t-\tau)}\mathrm{d}\tau \\ &+ \int_{-\infty}^{\infty} \tilde{w}(t-\tau)p^*(-\tau)\mathrm{d}\tau. \end{aligned} \tag{2.3}$$

Assuming PN does not change over the symbol duration, but changes from one symbol to another so that no intersymbol interference arises, sampling the matched filter output (2.3) at nT time instants results in

$$y(nT) = s[n]e^{j\phi(nT)} + w(nT). \tag{2.4}$$

We change the notation as

$$y[n] = s[n]e^{j\phi[n]} + w[n], \tag{2.5}$$

where $\phi[n]$ represents the PN of the nth received symbol in the digital domain that is bandlimited after the matched filter, and $w[n]$ is the filtered (bandlimited) and sampled version of $\tilde{w}(t)$ that is a zero-mean circularly symmetric complex-valued AWGN with variance σ_w^2. Note that in this work our focus is on oscillator phase synchronization and time synchronization is assumed to be perfect.

The slow varying PN assumption and the introduced discrete-time model (2.5), are well accepted in related literature (e.g., [8,9,18–30]). We also refer the reader to the recent studies of this model where the PN variations over the symbol period has also been taken into consideration, and the possible loss due to the slow varying PN approximation has been investigated [31–33].

3 Effect of Phase Noise on Communication Systems

As we saw in the previous section in Eq. 2.5, PN destroys the transmitted signals. Random rotation of the received signal constellation [18, 22, 30], and spectrum regrowth [8, 9, 20, 23, 34] are the main effects of this phenomenon on the communication systems.

3.1 Rotation of the Constellation Diagram

PN results in random rotation of the received signal constellation, which in phase modulated transmissions may lead to symbol detection errors [18, 22, 30].

Fig. 2.2a illustrates the received signal constellation of a system employing 16-QAM modulation format over an AWGN channel. Fig. 2.2b, on the other hand shows the effect of PN from a free-running oscillator on the received signal constellation. The rotatory distortions are due to the random variation of the phase of the received signal. The dashed lines show the Voronoi regions of a coherent detector, designed for the AWGN channel. PN cause decision errors by moving the received signals to wrong decision regions.

Fig. 2.3 shows the effect of PN before compensation on symbol error rate (SER) of the system, where it is compared against the SER in case of AWGN.

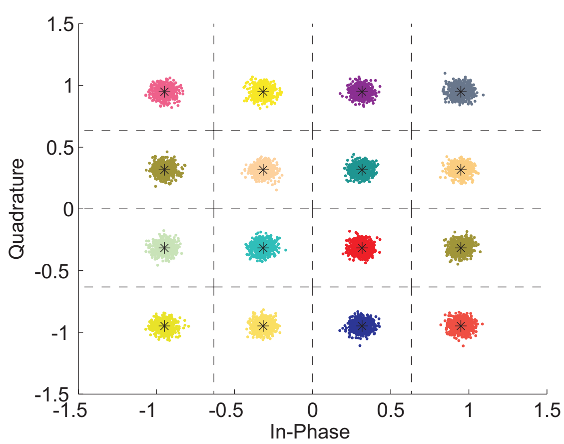

(a)

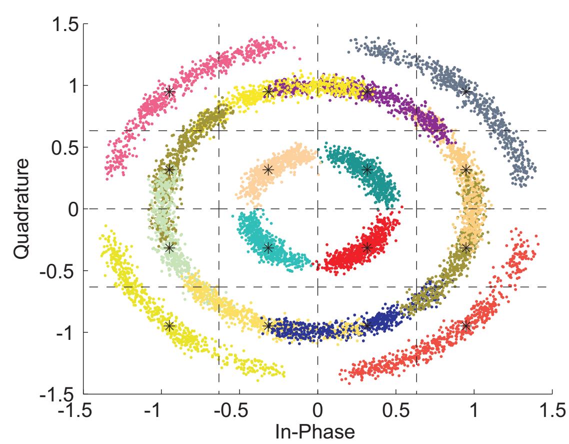

(b)

Figure 2.2: Received signal constellation of a 16-QAM system. (a) Pure AWGN channel with SNR=25 dB. (b) AWGN channel affected by PN, SNR=25 dB and PN increment variance of 10^{-4} rad^2/symbol duration.

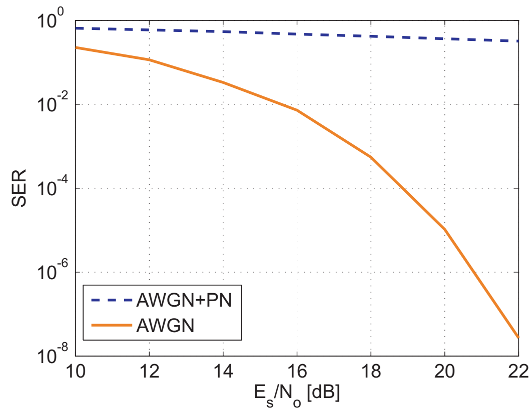

Figure 2.3: Effect of PN before compensation on the SER of a 16-QAM system.

3.2 Spectral Regrowth

PN may result in spectral regrowth, which can further cause adjacent channel interference in frequency division multiplexing systems [35, 36]. Fig. 2.4a shows two systems with the bandwidth of 22 MHz, and central frequencies of 2.412 and 2.437 GHz. Both systems use low-PN oscillators which results in no overlapping between the bands. On the other hand, Fig. 2.4b illustrates a case where the first system employs a noisy oscillator that cause power leakage to the other band resulting interchannel channel interference.

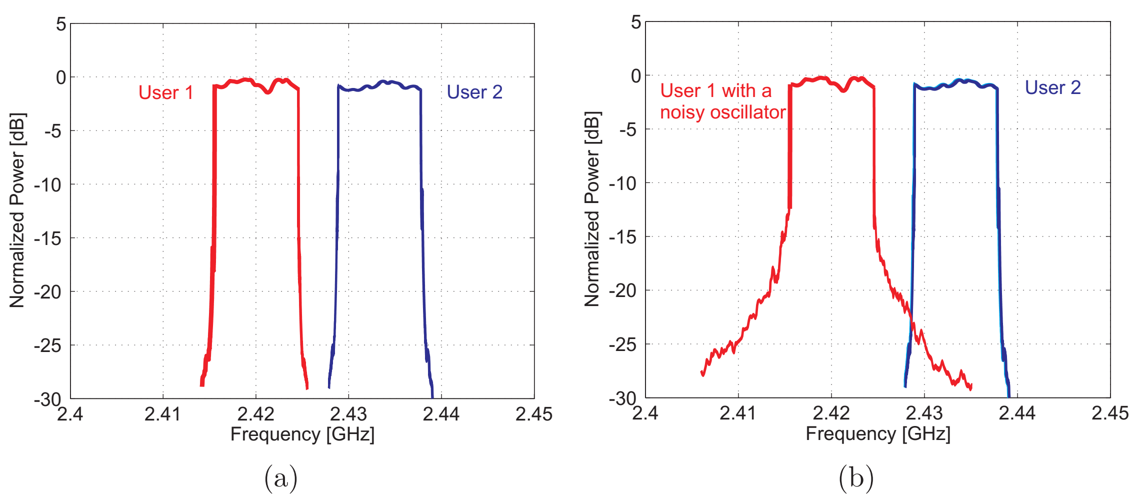

Figure 2.4: Effect of using ideal or noisy oscillators on the spectrum. (a) Two systems employing low PN oscillators. (b) Two systems, one using a noisy oscillator, which interferes with the other channel by spectrum regrowth.

CHAPTER 3

PHASE NOISE IN OSCILLATORS

1 Oscillators

Oscillators are autonomous systems, which provide a reference signal for frequency and timing synchronization. Harmonic oscillators with sinusoidal output signals are used for up-conversion of the baseband signal to an intermediate/radio frequency signal at the transmitters, and down-conversion from radio frequencies to baseband at the receivers (see Fig. 2.1).

Fig. 3.1 illustrates the block diagram of a feedback oscillator consisting of an amplifier and a feedback network. Roughly speaking, the oscillation mechanism is based on positive feedback of a portion of the output signal to the input of the amplifier through the feedback network [37].

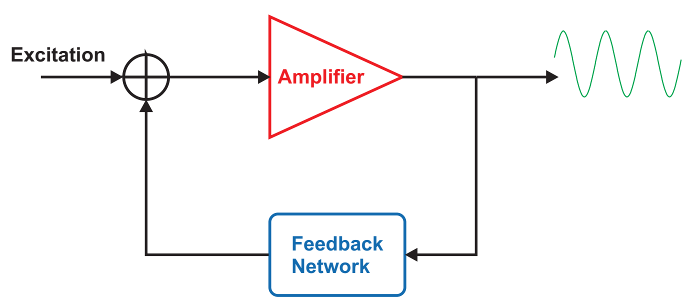

Figure 3.1: Block diagram of a typical feedback oscillator.

The feedback network is a resonator circuit, e.g., an LC network, and the amplifier is normally composed of diodes or transistors. One of the main sources of PN in the output oscillatory signal is the noise of such internal electronic devices.

2 Phase Noise in Oscillators

In an ideal oscillator, the phase transition over a given time interval is constant and the output signal is perfectly periodic. However in practical oscillators, the amount of phase increment is a random variable. This phase variation is called PN increment or phase jitter, and the instantaneous deviation of the phase from the ideal value is called PN [11, 16, 35].

In time domain, the output of a harmonic oscillator with normalized amplitude can be expressed as

$$v(t) = (1 + a(t)) \cos (2\pi f_0 t + \phi(t)) , \tag{3.1}$$

where f_0 is the oscillator's central frequency, and $a(t)$ and $\phi(t)$ denote the amplitude noise and PN processes, respectively [11]. The amplitude noise and PN are modeled as two independent random processes. According to [11, 38] the amplitude noise has insignificant effect on the output signal of the oscillator. Thus hereinafter, the effect of amplitude noise is neglected and the focus is on the study of the PN process.

Fig. 3.2 compares the output signal of an ideal oscillator with a noisy one. It can be seen that in the output of the noisy oscillator, the zero crossing time randomly changes due to PN.

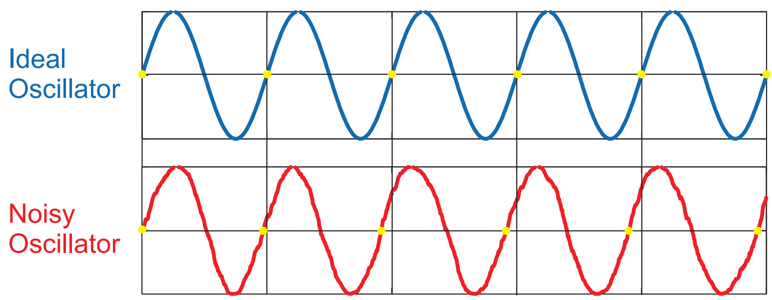

Figure 3.2: Effect of PN on the output oscillatory signal.

For an ideal oscillator where the whole power is concentrated at the central frequency f_0, the power spectral density would be a Dirac delta function, while in reality, PN results in spreading the power over frequencies around f_0 (Fig. 3.3).

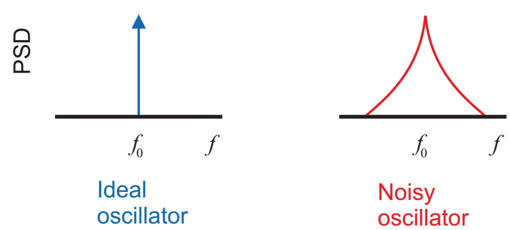

Figure 3.3: Effect of phase noise on the oscillator's power spectral density.

In frequency domain, PN is most often characterized in terms of single-side-band (SSB) PN spectrum [10, 11], defined as

$$\mathcal{L}(f) = \frac{P_{\mathrm{SSB}}(f_0 + f)}{P_{\mathrm{Total}}}, \tag{3.2}$$

where $P_{\mathrm{SSB}}(f_0 + f)$ is the single-side-band power of oscillator within 1 Hz bandwidth around the offset frequency f from the central frequency f_0, and P_{Total} is the total power of the oscillator.

By plotting the experimental measurements of free running oscillators on a logarithmic scale, it is possible to see that $\mathcal{L}(f)$ usually follows slopes of -30 dB/decade and -20 dB/decade, until a flat noise floor is reached at higher frequency offsets. Fig. 3.4 shows the measured SSB PN spectrums from a GaN HEMT MMIC oscillator.

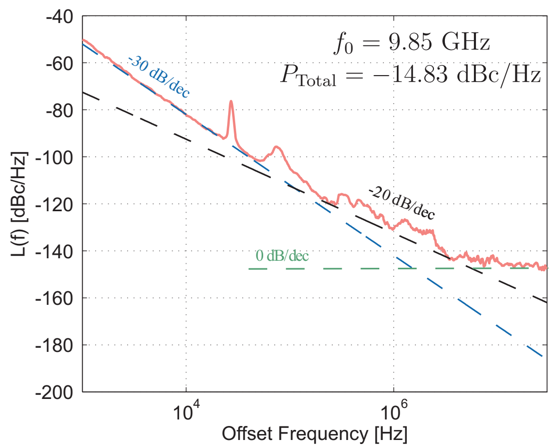

Figure 3.4: The SSB PN spectrum from a GaN HEMT MMIC oscillator. Drain voltage $V_{\text{dd}} = 6$ V and drain current $I_{\text{d}} = 30$ mA.

3 Phase Noise Generation

Oscillator PN originates from the noise inside the circuitry. The internal noise sources can be categorized as white (uncorrelated) and colored (correlated) noise sources [10, 11, 39]. A white noise process has a flat power spectral density (PSD), which is not the case for colored noise sources. Noise sources such as thermal noise inside the devices are modeled as white, while substrate and supply-noise sources, as well as low-frequency noise, are modeled as colored sources. A significant part of the colored noise sources inside the circuit can be modeled as flicker noise [11]. Fig. 3.5, shows a typical PSD of the noise sources inside the oscillator circuitry, plotted on a logarithmic scale.

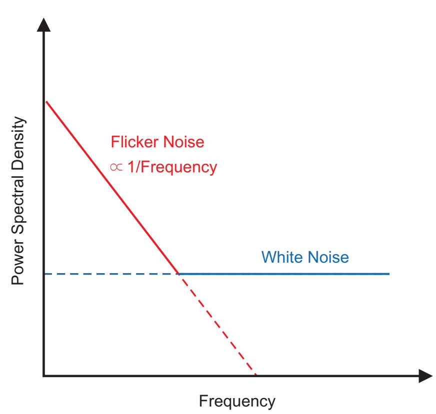

Figure 3.5: Power spectral density of noise inside the oscillator circuitry, plotted on a logarithmic scale.

The PN generation mechanism in the oscillator is usually explained as the integration of the white and colored noise sources [10, 39]. However, this cannot describe the entire frequency properties of the practical oscillators. Hence, we consider a more general model in our analysis, where PN is partially generated from the integration of the circuit noise, and the rest is a result of amplification/attenuation of the noise inside the circuitry. For example, PN with -30 and -20 dB/decade slopes originate from integration of flicker noise (colored noise) and white noise, respectively. The flat noise floor, also known as white PN originates directly from the thermal noise. Fig. 3.6 illustrates the PN generation mechanism.

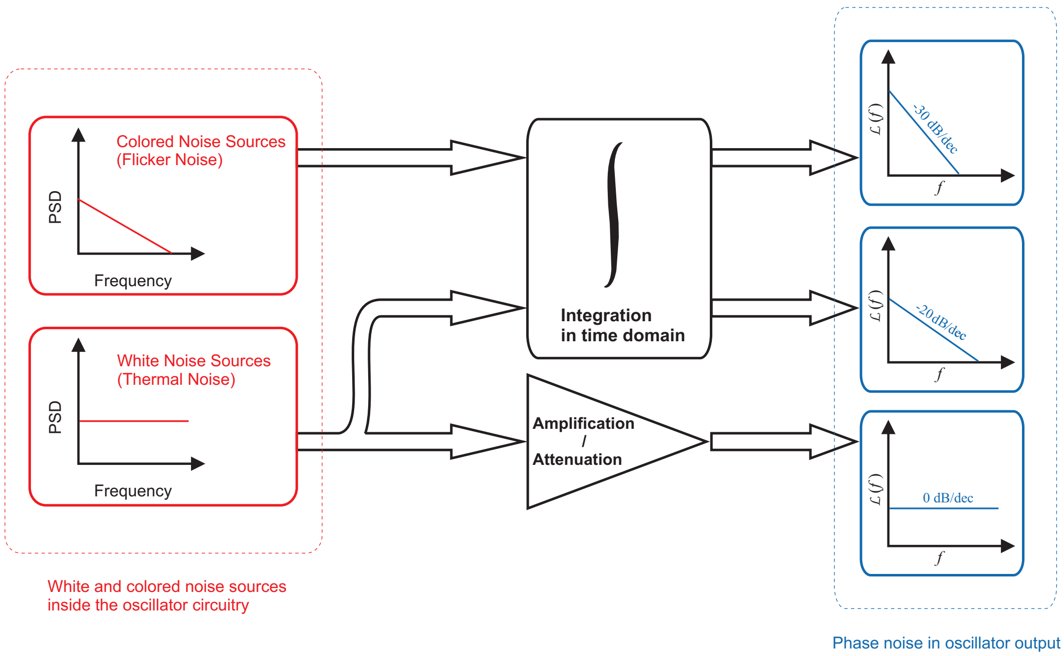

Figure 3.6: Phase noise generation mechanism.

In our analysis we are interested in the PSD of the PN process denoted as $S_\phi(f)$. It is possible to show that in high offset frequencies, $S_\phi(f)$ is well approximated with $\mathcal{L}(f)$ that is the normalized PSD of the oscillator [10, 40, 41],

$$S_\phi(f) \approx \mathcal{L}(f) \text{ for large } f. \tag{3.3}$$

The offset frequency range where this approximation is valid depends on the PN performance of the studied oscillator [42]. It can be shown that the final system performance is not sensitive to low frequency offsets. Thus for low frequency offsets, $S_\phi(f)$ can be modeled in such a way that it follows the same slope as that of higher frequencies [15].

4 Phase Noise Modeling

In order to study the effect of PN and design of algorithms for mitigation of its effects, models that can accurately capture the characteristics of this phenomenon are required. In most prior studies, the effects of PN are studied using simple models, e.g, the Wiener process [10, 12, 24, 26, 27, 30–33]. The Wiener process does not take into account colored noise sources [39] and hence cannot describe frequency and time-domain properties of PN properly [12, 13, 15, 43]. This motivates use of more realistic PN models in study and design of communication systems. In this thesis we consider the effect of both white and colored noise sources. Assuming independent noise sources, PN can be modeled as a superposition of three independent processes

$$\phi(t) = \phi_3(t) + \phi_2(t) + \phi_0(t), \tag{3.4}$$

where $\phi_3(t)$ and $\phi_2(t)$ model PN with -30 and -20 dB/decade slopes in the PSD that originate from integration of flicker noise (colored noise) and white noise, denoted as $\Phi_3(t)$ and $\Phi_2(t)$, respectively:

$$\phi_3(t) = \int_0^t \Phi_3(\tau)\mathrm{d}\tau, \qquad \phi_2(t) = \int_0^t \Phi_2(\tau)\mathrm{d}\tau. \tag{3.5}$$

Further, $\phi_0(t)$ models the flat noise floor, which is the direct effect of white thermal noise of the circuit.

Due to the integration, processes $\phi_3(t)$ and $\phi_2(t)$ have a *cumulative* nature [10, 40]; PN accumulation over the time delay T is modeled as a random process. This process is usually called the PN increment process [15], self-referenced PN [44], or the differential PN process [45] that mathematically defined as

$$\zeta_2(t,T) = \phi_2(t) - \phi_2(t-T) = \int_{t-T}^t \Phi_2(\tau)\mathrm{d}\tau, \tag{3.6a}$$

$$\zeta_3(t,T) = \phi_3(t) - \phi_3(t-T) = \int_{t-T}^t \Phi_3(\tau)\mathrm{d}\tau. \tag{3.6b}$$

It has been shown in several studies that the PN increment process can be accurately modeled as a zero-mean Gaussian stationary process [10, 44]. In order to evaluate this model in practice, we examine the time-domain measurements of a GaN HEMT MMIC oscillator. Histograms of two time-separated frames of PN increment samples from this oscillator, are compared in Fig. 3.7. This observation shows that the PN increments can be reasonably well modeled with a Gaussian distribution. It can also be seen that the mean and variance of the samples within the frames are almost equal and do not change over time.

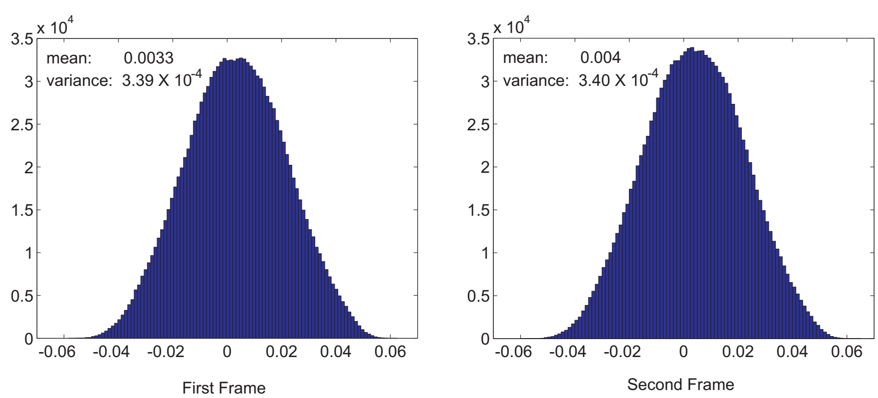

Figure 3.7: Histograms of two time-separated frames of PN increment samples from a GaN HEMT MMIC oscillator.

The statistical correlations of the PN increments depend on the correlation properties of the noise sources inside the oscillator. The white noise sources result in uncorrelated PN increments, while the PN increments from the colored noise sources are correlated [10, 12–15].

In many practical systems, the free running oscillator is stabilized inside a phase-locked loop (PLL). A PLL architecture that is widely used in frequency synchronization consists of a free-running oscillator, a reference oscillator, a loop filter, phase-frequency detectors and frequency dividers [10, 44, 46, 47]. Any of these components may contribute to the output PN of the PLL. It is reasonable to assume that PN of the free-running oscillator has the most dominant effect on the output of a PLL [10, 44]. A PLL behaves as a high-pass filter for the free-running oscillator's PN. Above a certain frequency, the PSD of the PLL output is identical to the PN PSD of the free-running oscillator, while below this frequency it approaches a constant value [10, 44, 46, 47].

Fig. 3.8 shows this spectrum model for a free and a PLL locked oscillator.

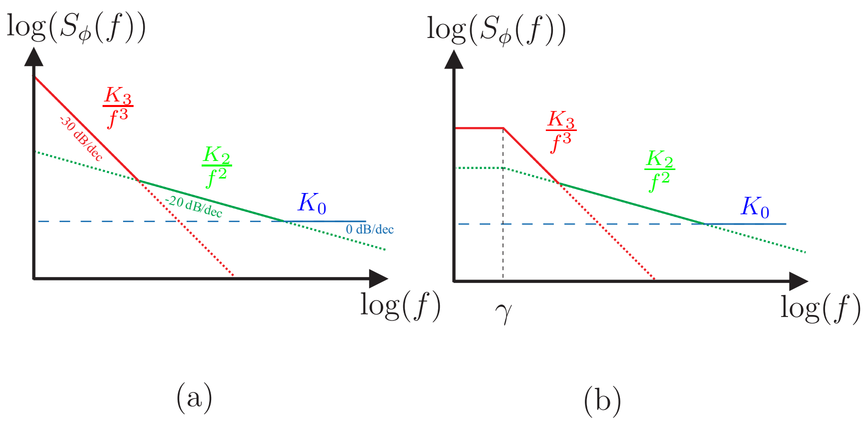

Figure 3.8: Phase noise PSD of a typical oscillator. (a) shows the PSD of a free running oscillator. (b) is a model for the PSD of a locked oscillator, where γ is the PLL loop's bandwidth. It is considered that the PN of the reference oscillator is negligible compared to the PN of the free running oscillator in the PLL.

In general for both free-running and PLL-stabilized oscillators, we model the PSD of $\phi_3(t)$, $\phi_2(t)$, and $\phi_0(t)$ as modified power-law spectrums [40]:

$$S_{\phi_3}(f) = \frac{K_3}{\gamma^3 + f^3}, \quad S_{\phi_2}(f) = \frac{K_2}{\gamma^2 + f^2}, \quad S_{\phi_0}(f) = K_0, \tag{3.7}$$

where K_3, K_2 and K_0 are the PSD levels and γ is a low cut-off frequency.

The performance of a PN-affected communication systems depends on the statistics of PN. In **Paper A**, we derive the required PN statistics from the proposed PN spectrum model (3.7). Some of the preliminaries and results are presented in the following.

4.1 Variance of the White Phase Noise Process

According to (3.7), the PSD of the white phase noise process denoted as $\phi_0(t)$ is defined as

$$S_{\phi_0}(f) = K_0, \tag{3.8}$$

where K_0 is the level of the noise floor that can be found from the measurements, and it is normalized with the oscillator power [48]. The system bandwidth is equal to the symbol rate $1/T$. At the receiver, a low-pass filter with the same bandwidth is applied to the received signal. According to [49], if K_0/T is small (which is generally the case in practice), low-pass filtering of the received signal results in filtering of $\phi_0(t)$ with the same bandwidth. Therefore we are interested in the PN process that is inside the system bandwidth. The variance of the bandlimited $\phi_0(t)$ is calculated as

$$\sigma^2_{\phi_0} = \int_{-1/2T}^{+1/2T} S_{\phi_0}(f)\mathrm{d}f = \frac{K_0}{T}. \tag{3.9}$$

As $\phi_0(t)$ is bandlimited, we can sample it without any aliasing.

4.2 Statistics of the Cumulative PN Increments

In many prior studies, focus has been on mathematical calculation of the variance of the PN increments from the spectrum measurements. It has been shown that for a free running oscillator, variance of $\zeta_3(t,T)$ and $\zeta_2(t,T)$, defined in (3.6a), over the time delay T is proportional to T and T^2, respectively [10, 50, 51].

Based on our analysis, PN increments can be correlated in the case of using an oscillator with colored noise sources. Moreover, we observe that the PN increments of a PLL-stabilized oscillator are correlated. Hence, both the variance and correlation of PN increments are required for accurate study of the cumulative PN.

In **Paper A**, we have shown that in general, for a PN process with PSD of $S_\phi(f)$, the autocorrelation function of PN increments can be calculated as

$$R_\zeta(\tau) = 8\int_0^{+\infty} S_\phi(f)\sin(\pi f T)^2\cos(2\pi f\tau)\mathrm{d}f, \tag{3.10}$$

where τ is the time lag parameter. In discrete-time domain, samples of $\zeta_3(t,T)$ and $\zeta_2(t,T)$ are denoted as $\zeta_3[m] \triangleq \zeta_3(mT,T)$ and $\zeta_2[m] \triangleq \zeta_2(mT,T)$, respectively, where T is equal to the sampling time, and m is the discrete-time index.

Employing (3.7) and (3.10), the autocorrelation function of $\zeta_2[m]$ is computed as

$$R_{\zeta_2}[m] = \frac{K_2\pi}{\gamma}\left(2e^{-2\gamma\pi T|m|} - e^{-2\gamma\pi T|m-1|} - e^{-2\gamma\pi T|m+1|}\right), \tag{3.11}$$

where K_2 is the PSD level and can be found from the measured spectrum. For a PLL-stabilized oscillator γ can be set to the PLL bandwidth, and for a free-running oscillator, the autocorrelation function can be found by taking the limit of (3.11) as γ approaches 0 that results in

$$R_{\zeta_2}[m] = \begin{cases} 4K_2\pi^2 T & \text{if } m = 0 \\ 0 & \text{otherwise} \end{cases}. \tag{3.12}$$

Results in (3.11) and (3.12) show that for a PLL-stabilized oscillator samples of $\zeta_2[n]$ process are correlated over time, while they are uncorrelated for a free-running oscillator. Fig. 3.9 compares $R_{\zeta_2}[m]$ of a free-running and a PLL-stabilized oscillator. The PN PSD level is $K_2 = 25$ rad^2 Hz, sampling time $T = 10^{-6}$ sec, and the PLL bandwidth $\gamma = 1$ MHz.

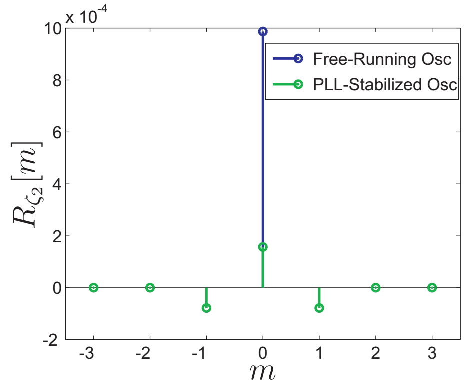

Figure 3.9: The autocorrelation function of $\zeta_2[m]$ for a free-running and PLL-stabilized oscillator.

Furthermore, by using (3.7) and (3.10), the autocorrelation function of $\zeta_3[m]$ is computed in **Paper A** as

$$R_{\zeta_3}[m] = \begin{cases} -8K_3\pi^2T^2\left(\Lambda + \log(2\pi\gamma T)\right), & \text{if } m = 0 \\ -8K_3\pi^2T^2(\Lambda + \log(8\pi\gamma T)), & \text{if } m = \pm 1 \\ -8K_3\pi^2T^2\Big[-m^2(\Lambda + \log(2\pi\gamma T|m|)) & \\ \qquad +\dfrac{(m+1)^2}{2}(\Lambda + \log(2\pi\gamma T|m+1|)) & \text{otherwise} \\ \qquad +\dfrac{(m-1)^2}{2}(\Lambda + \log(2\pi\gamma T|m-1|))\Big], & \end{cases} \tag{3.13}$$

where $\Lambda \triangleq \Gamma - 3/2$, and $\Gamma \approx 0.5772$ is the Euler-Mascheroni constant [52], K_3 can be found from the measurements. The cut-off frequency γ must be set to a small value for a free running oscillator, while for a PLL-stabilized oscillator it can be set to the PLL bandwidth. Fig. 3.10 shows the evaluated $R_{\zeta_3}[m]$ for a free-running oscillator. It can be observed that the samples of $\zeta_3[m]$ are highly correlated.

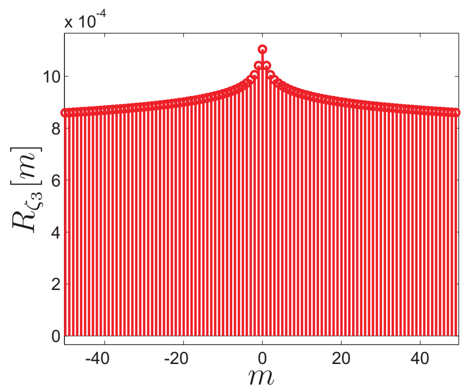

Figure 3.10: Autocorrelation of $\zeta_3[m]$, showing the samples are highly correlated.

CHAPTER 4

PHASE NOISE COMPENSATION

1 Overview

Design of communication systems in presence of PN has been an active field of research during the last decades. The ultimate goal of such studies is to achieve a performance close to that of the coherent systems. Various system-level architectures for the receiver of communication systems have been proposed, and many of them are based on estimation of PN in the digital domain. The estimator provides an estimated value or statistics of the PN that can further be used for symbol detection. For example, estimation of the PN and cleaning the received signal, followed by a coherent detector is proposed in [53]. In [30] on the other hand, a joint PN estimation-symbol detection algorithm based on iterative interactions of PN estimator and symbol detector is suggested. Fig. 4.1 shows the simplified receiver of a communication system, designed for the PN channel.

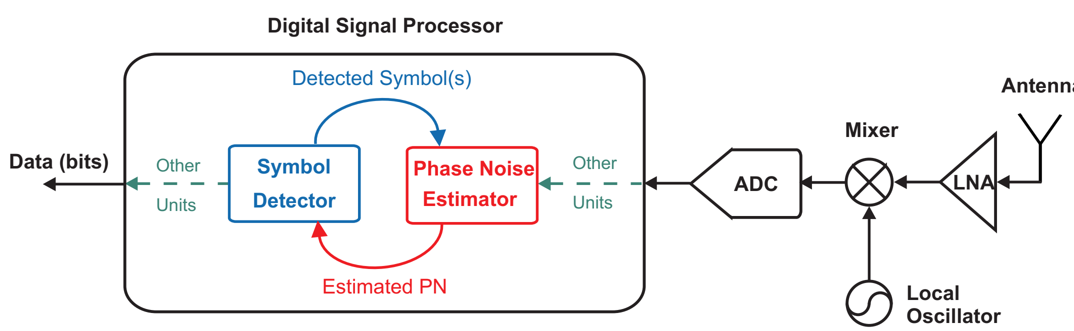

Figure 4.1: Receiver of a communication system designed for the PN channel.

Several algorithms for PN estimation based on deterministic or statistical approaches have been proposed. In many of the former studies, PN has been modeled as a discrete-time Wiener process [12, 24, 26, 27, 30–33], while it is only accurate for oscillators with white noise sources [10, 15, 43].

In this thesis we focus on estimation of PN with colored and white noise sources. We propose statistical algorithms for PN estimation based on Bayesian approaches. The proposed PN estimators employ the received signal and the a priori known statistics of the PN process to perform the estimation. The estimated PN value, denoted as $\hat{\phi}[n]$, is used to de-rotate and clean the received signal introduced in Chapt. 2, Eq. (2.5). The de-rotated received signal can be written as

$$\dot{y}[n] = s[n]e^{j(\phi[n]-\hat{\phi}[n])} + \dot{w}[n], \tag{4.1}$$

where $\dot{w}[n] \triangleq e^{-j\phi[n]}w[n]$ has the same statistics as $w[n]$. The main design criterion for such an estimator is to minimize a function of the PN estimation error $(\phi[n]-\hat{\phi}[n])$ which is called a cost function.

In the following, we start with a brief overview of the Bayesian estimation and present our methods for estimation of PN with colored noise sources.

2 Bayesian Framework

In the Bayesian framework, unknown parameters are considered as random. The Bayesian approach perfectly fits the PN estimation problem, because PN is a random phenomenon by its physical nature. In Bayesian analysis, the knowledge about the random parameter of interest is mathematically summarized in a prior distribution. In PN inference problems, the prior distribution can be chosen subjectively by studying the physical characteristics of this phenomenon. This further motivates the accurate statistical modeling of the PN.

2.1 Bayesian Estimation

The ultimate goal in Bayesian estimation is to find an estimate that minimizes a Bayesian risk function [54]. The Bayesian risk functions are usually defined as the expectation of a specific cost functions. In this thesis, we are mainly interested in quadratic and uniform (hit-or-miss) cost functions [54, 55]. The minimizer of the quadratic risk is called the Bayesian minimum mean square error (MMSE) estimator, and it is possible to show that this estimator is equal to the mean of the posteriori distribution. Kalman filter is an example of MMSE estimators [55]. Further, the minimizer of the uniform risk is equal to the mode of the posteriori distribution and it is called maximum a posteriori (MAP) estimator.

In particular, when the linear Gaussian model is adopted, the mean and the mode of the posterior distribution are identical and the MAP estimator performs similar to the MMSE estimator. There are other special scenarios where the MAP estimator also minimizes the quadratic risk function and it is optimal in the MMSE sense.

2.2 Estimation of Phase Noise with Colored Noise Sources

In **Paper B**, we study the design of algorithms for estimation of PN with colored noise sources. The proposed algorithms are employed for estimation of PN from realistic oscillators. The PN samples are modeled by a random-walk with correlated samples. Based on the results of **Paper A**, we calculate the autocorrelation function of the PN increments from the PN spectrum measurements. Two algorithms, a MAP estimator and a modified

Kalman smoother (Rauch–Tung–Striebel smoother [56]) are proposed for estimation of PN with colored increments. Because the data symbols are not known to the PN estimators, an iterative PN estimation algorithm is employed, where first the known pilot symbols are used to find an initial estimate of the PN samples. Then, the estimation is improved by using the statistics of the soft-detected symbols from the symbol detector.

3 Performance of Bayesian Estimators

3.1 Bayesian Cramér Rao Bound

In order to assess the estimation performance, Cramér-Rao bounds (CRBs) can be utilized, which give a lower bound on the mean square error (MSE) of parameter estimation [55]. In the case of random parameter estimation, e.g., PN estimation, the Bayesian Cramér-Rao bound (BCRB) gives a tight lower bound on the MSE [54].

Consider the estimation of a vector of PN samples with length N denoted as $\boldsymbol{\varphi} = [\phi[1], \ldots, \phi[N]]^T$. The BCRB bounds the covariance matrix of the estimation error by the following inequality

$$\mathbb{E}\left[(\hat{\boldsymbol{\varphi}} - \boldsymbol{\varphi})(\hat{\boldsymbol{\varphi}} - \boldsymbol{\varphi})^T\right] \geq \mathbf{BCRB}, \tag{4.2}$$

$$\mathbf{BCRB} = \mathbf{B}^{-1}, \tag{4.3}$$

where $\mathbf{B}$ is called Bayesian information matrix (BIM). The BIM is calculated in two parts, $\mathbf{B} = \boldsymbol{\Xi} + \boldsymbol{\Psi}$, where $\boldsymbol{\Xi}$ is derived from the likelihood function and $\boldsymbol{\Psi}$ from the prior distribution function of $\boldsymbol{\varphi}$. In **Paper A**, we have derived the BCRB for estimation of PN with colored noise sources. The calculated BCRB directly depends on the calculated statistics of PN from the measurements through the prior distribution of PN vector.

CHAPTER 5

CONCLUSIONS, CONTRIBUTIONS, AND FUTURE WORK

1 Conclusions

In this thesis we study different aspects of the problem of PN in communication systems. First, we derive statistics of PN in real oscillators. Then, we employ those statistics for design of PN estimation algorithms, as well as calculation of the performance of PN-affected communication systems.

We are now ready to summarize and conclude our contributions.

2 Contribution

The contribution of the appended papers are shortly described in the following.

Paper A: Calculation of the Performance of Communication Systems from Measured Oscillator Phase Noise

In this paper, we investigate the relation between real oscillator PN measurements and the performance of communication systems. To this end, we first derive statistics of PN with white and colored noise sources in free-running and PLL-stabilized oscillators. Based on the calculated statistics, analytical BCRB for estimation of phase noise with white and colored sources is derived. Finally, the system performance in terms of error vector magnitude of the received constellation is computed from the calculated BCRB.

According to our analysis, the influence from different noise regions strongly depends on the communication bandwidth, i.e., the symbol rate. For example, in high symbol rate communication systems, cumulative PN that appears near carrier is of relatively low importance compared to the white PN far from carrier.

The paper's findings can be used by hardware and frequency generator designers to better understand the effect of phase noise with different sources on the system performance and optimize their design criteria respectively. Moreover, the computed PN statistics can further be used in design of PN estimation algorithms.

Paper B: Estimation of Phase Noise in Oscillators with Colored Noise Sources

In this work design of algorithms for estimation of PN with colored noise sources is studied. A soft-input maximum a posteriori PN estimator and a modified soft-input extended Kalman smoother are proposed.

We show that deriving the soft-input MAP estimator is a concave optimization problem at moderate and high SNRs. To be able to implement the Kalman algorithm for filtering/smoothing of PN with colored increments, the state equation is modified by means of an autoregressive modeling.

The performance of the proposed algorithms is compared against those studied in the literature, in terms of mean square error of PN estimation, and symbol error rate of the considered communication system. The comparisons show that considerable performance gains can be achieved by designing estimators that employ correct knowledge of the PN statistics. The gain is more significant in low-SNR or low-pilot density scenarios.

3 Future Work

In the following, we have described some of our ongoing studies and possible future research directions.

Currently we are working on calculation of the Shannon capacity of the PN channel directly from the real oscillator measurements. Such results would be useful to study the effect of different noise sources on the ultimate number of bits that can be transmitted through this channel. Further, they can be used by hardware and system designers to optimize their implementations.

We are also exploring the effects of PN with both white and colored sources on MIMO communication systems. Another area that we intend to study is the effect of PN on reciprocal communication systems. It is also of interest to adopt our algorithms for compensation of PN in multi-carrier communication systems.

References

[1] R. W. Tkach, "Scaling optical communications for the next decade and beyond," *Bell Labs Tech. J.*, vol. 14, no. 4, pp. 3–9, 2010.

[2] T. Schenk and J.-P. Linnartz, *RF imperfections in high-rate wireless systems: impact and digital compensation.* Springer, 2008.

[3] P. Smulders, "Exploiting the 60 GHz band for local wireless multimedia access: prospects and future directions," *IEEE Commun. Mag.*, vol. 40, no. 1, pp. 140–147, 2002.

[4] Y. Li, H. Jacobsson, M. Bao, and T. Lewin, "High-frequency SiGe MMICs-an industrial perspective," *Proc. GigaHertz 2003 Symp.,* Linköping, Sweden, Nov. 2003.

[5] M. Dohler, R. Heath, A. Lozano, C. Papadias, and R. Valenzuela, "Is the PHY layer dead?" *IEEE Commun. Mag.*, vol. 49, no. 4, pp. 159 –165, Apr. 2011.

[6] G. Durisi, A. Tarable, and T. Koch, "On the multiplexing gain of MIMO microwave backhaul links affected by phase noise," *Proc. IEEE Int. Conf. Commun.(ICC)*, Jun. 2013.

[7] M.R. Khanzadi, R. Krishnan, and T. Eriksson, "Effect of synchronizing coordinated base stations on phase noise estimation," *Proc. IEEE Acoust., Speech, Signal Process. (ICASSP)*, May. 2013.

[8] L. Tomba, "On the effect of Wiener phase noise in OFDM systems," *IEEE Trans. Commun.*, vol. 46, no. 5, pp. 580 –583, 1998.

[9] F. Munier, T. Eriksson, and A. Svensson, "An ICI reduction scheme for OFDM system with phase noise over fading channels," *IEEE Trans. Commun.*, vol. 56, no. 7, pp. 1119 –1126, 2008.

[10] A. Demir, "Computing timing jitter from phase noise spectra for oscillators and phase-locked loops with white and $1/f$ noise," *IEEE Trans. Circuits Syst. I, Reg. Papers*, vol. 53, no. 9, pp. 1869 –1884, Sep. 2006.

[11] A. Hajimiri and T. Lee, "A general theory of phase noise in electrical oscillators," *IEEE J. Solid-State Circuits*, vol. 33, no. 2, pp. 179 –194, 1998.

[12] M.R. Khanzadi, H. Mehrpouyan, E. Alpman, T. Svensson, D. Kuylenstierna, and T. Eriksson, "On models, bounds, and estimation algorithms for time-varying phase noise," *Int. Conf. Signal Process. Commun. Syst. (ICSPCS)*, pp. 1 –8, Dec. 2011.

[13] M.R. Khanzadi, A. Panahi, D. Kuylenstierna, and T. Eriksson, "A model-based analysis of phase jitter in RF oscillators," *IEEE Intl. Frequency Control Symp. (IFCS)*, pp. 1 –4, May 2012.

[14] M.R. Khanzadi, R. Krishnan, and T. Eriksson, "Estimation of phase noise in oscillators with colored noise sources," *Accepted for publication in IEEE Commun. Lett.*, Aug. 2013.

[15] M.R. Khanzadi, D. Kuylenstierna, A. Panahi, T. Eriksson, and H. Zirath, "Calculation of the performance of communication systems from measured oscillator phase noise," *Accepted for publication in IEEE Trans. Circuits Syst. I, Reg. Papers*, Aug. 2013.

[16] A. Demir, A. Mehrotra, and J. Roychowdhury, "Phase noise in oscillators: a unifying theory and numerical methods for characterization," *IEEE Trans. Circuits Syst. I, Fundam. Theory Appl.*, vol. 47, no. 5, pp. 655 –674, May 2000.

[17] J. G. Proakis and M. Salehi,, *Digital communications*, 5th ed. New York: McGraw-Hill, 2008.

[18] H. Meyr, M. Moeneclaey, and S. Fechtel, *Digital Communication Receivers: Synchronization, Channel Estimation, and Signal Processing*. New York, NY, USA: John Wiley & Sons, Inc., 1997.

[19] A. Armada and M. Calvo, "Phase noise and sub-carrier spacing effects on the performance of an OFDM communication system," *IEEE Commun. Lett.*, vol. 2, no. 1, pp. 11 –13, 1998.

[20] A. Armada, "Understanding the effects of phase noise in orthogonal frequency division multiplexing (OFDM)," *IEEE Trans. Broadcast.*, vol. 47, no. 2, pp. 153 –159, Jun. 2001.

[21] P. Amblard, J. Brossier, and E. Moisan, "Phase tracking: what do we gain from optimality? particle filtering versus phase-locked loops," *Elsevier Signal Process.*, vol. 83, no. 1, pp. 151 – 167, Mar. 2003.

[22] F. Munier, E. Alpman, T. Eriksson, A. Svensson, and H. Zirath, "Estimation of phase noise for QPSK modulation over AWGN channels," *Proc. GigaHertz 2003 Symp.,* Linköping, Sweden, Nov. 2003.

[23] S. Wu and Y. Bar-Ness, "OFDM systems in the presence of phase noise: consequences and solutions," *IEEE Trans. Commun.*, vol. 52, no. 11, pp. 1988 – 1996, Nov. 2004.

[24] G. Colavolpe, A. Barbieri, and G. Caire, "Algorithms for iterative decoding in the presence of strong phase noise," *IEEE J. Sel. Areas Commun.*, vol. 23, pp. 1748–1757, Sep. 2005.

[25] M. Nissila and S. Pasupathy, "Adaptive iterative detectors for phase-uncertain channels via variational bounding," *IEEE Trans. Commun.*, vol. 57, no. 3, pp. 716 –725, Mar. 2009.

[26] R. Krishnan, H. Mehrpouyan, T. Eriksson, and T. Svensson, "Optimal and approximate methods for detection of uncoded data with carrier phase noise," *IEEE Global Commun. Conf. (GLOBECOM)*, pp. 1 –6, Dec. 2011.

[27] R. Krishnan, M.R. Khanzadi, L. Svensson, T. Eriksson, and T. Svensson, "Variational bayesian framework for receiver design in the presence of phase noise in MIMO systems," *IEEE Wireless Commun. and Netw. Conf. (WCNC)*, pp. 1 –6, Apr. 2012.

[28] H. Mehrpouyan, A. A. Nasir, S. D. Blostein, T. Eriksson, G. K. Karagiannidis, and T. Svensson, "Joint estimation of channel and oscillator phase noise in MIMO systems," *IEEE Trans. Signal Process.*, vol. 60, no. 9, pp. 4790 –4807, Sep. 2012.

[29] G. Durisi, A. Tarable, C. Camarda, and G. Montorsi, "On the capacity of MIMO Wiener phase-noise channels," *Proc. Inf. Theory Applicat. Workshop (ITA)*, Feb. 2013.

[30] R. Krishnan, M.R. Khanzadi, T. Eriksson, and T. Svensson, "Soft metrics and their performance analysis for optimal data detection in the presence of strong oscillator phase noise," *IEEE Trans. Commun.*, vol. 61, no. 6, pp. 2385 –2395, Jun. 2013.

[31] M. Martalò, C. Tripodi, and R. Raheli, "On the information rate of phase noise-limited communications," *Proc. Inf. Theory Applicat. Workshop (ITA)*, Feb. 2013.

[32] H. Ghozlan and G. Kramer, "On Wiener phase noise channels at high signal-to-noise ratio," *arXiv preprint arXiv:1301.6923*, 2013.

[33] ——, "Multi-sample receivers increase information rates for Wiener phase noise channels," *arXiv preprint arXiv:1303.6880*, 2013.

[34] T. Pollet, M. Van Bladel, and M. Moeneclaey, "BER sensitivity of OFDM systems to carrier frequency offset and Wiener phase noise," *IEEE Trans. Commun.*, vol. 43, no. 234, pp. 191 –193, Feb./Mar./Apr. 1995.

[35] A. A. Abidi, "How phase noise appears in oscillators," in *Analog Circuit Design.* Springer, 1997, pp. 271–290.

[36] E. Costa and S. Pupolin, "M-QAM-OFDM system performance in the presence of a nonlinear amplifier and phase noise," *IEEE Trans. Commun.*, vol. 50, no. 3, pp. 462–472, Aug. 2002.

[37] G. Gonzalez, *Foundations of oscillator circuit design.* Artech House Boston, MA, 2007.

[38] G. Klimovitch, "A nonlinear theory of near-carrier phase noise in free-running oscillators," *Proc. IEEE Intl. Conf. on Circuits Systs.*, pp. 1 –6, 2000.

[39] A. Demir, "Phase noise and timing jitter in oscillators with colored-noise sources," *IEEE Trans. Circuits Syst. I, Fundam. Theory Appl.*, vol. 49, no. 12, pp. 1782 – 1791, Dec. 2002.

[40] A. Chorti and M. Brookes, "A spectral model for RF oscillators with power-law phase noise," *IEEE Trans. Circuits Syst. I, Reg. Papers*, vol. 53, no. 9, pp. 1989 –1999, 2006.

[41] G. Klimovitch, "Near-carrier oscillator spectrum due to flicker and white noise," *Proc. IEEE Intl. Symp. on Circuits Systs.*, vol. 1, pp. 703 –706 vol.1, May 2000.

[42] T. Decker and R. Temple, "Choosing a phase noise measurement technique," *RF and Microwave Measurement Symposium and Exhibition*, 1999.

[43] S. Yousefi and J. Jalden, “On the predictability of phase noise modeled as flicker FM plus white FM,” *Proc. Asilomar Conf.*, pp. 1791 –1795, Nov. 2010.

[44] J. McNeill, “Jitter in ring oscillators,” Ph.D. dissertation, Boston University, 1994.

[45] A. Murat, P. Humblet, and J. Young, “Phase-noise-induced performance limits for DPSK modulation with and without frequency feedback,” *J. Lightw. Technol.*, vol. 11, no. 2, pp. 290 –302, Feb. 1993.

[46] K. Kundert, “Predicting the phase noise and jitter of PLL-based frequency synthesizers,” 2003, [Online]. Available: http://designers-guide.com.

[47] C. Liu, “Jitter in oscillators with $1/f$ noise sources and application to true RNG for cryptography,” Ph.D. dissertation, Worcester Polytechnic Institute, 2006.

[48] D. Leeson, “A simple model of feedback oscillator noise spectrum,” *Proc. IEEE*, vol. 54, no. 2, pp. 329 – 330, 1966.

[49] R. Corvaja and S. Pupolin, “Effects of phase noise spectral shape on the performance of DPSK systems for wireless applications,” *Eur. Trans. Telecommun. (ETT)*, vol. 13, no. 3, pp. 203–210, May. 2002. [Online]. Available: http://dx.doi.org/10.1002/ett.4460130305

[50] J. McNeill, “Jitter in ring oscillators,” *IEEE J. Solid-State Circuits*, vol. 32, no. 6, pp. 870 –879, Jun. 1997.

[51] C. Liu and J. McNeill, “Jitter in oscillators with $1/f$ noise sources,” *Proc. IEEE 2004 Intl. Symp. on Circuits Systs.*, vol. 1, pp. 773–776, May. 2004.

[52] J. Havil, *Gamma: exploring Euler’s constant*. Princeton, NJ: Princeton University Press, 2003.

[53] J. Bhatti and M. Moeneclaey, “Feedforward data-aided phase noise estimation from a DCT basis expansion,” *EURASIP J. Wirel. Commun. Netw.*, Jan. 2009.

[54] H. L. V. Trees, *Detection, Estimation and Modulation Theory*. New York: Wiley, 1968, vol. 1.

[55] S. M. Kay, *Fundamentals of Statistical Signal Processing, Estimation Theory*. Prentice Hall, Signal Processing Series, 1993.

[56] H. E. Rauch, C. Striebel, and F. Tung, “Maximum likelihood estimates of linear dynamic systems,” *AIAA J.*, vol. 3, no. 8, pp. 1445–1450, Aug. 1965.

Part II

Included papers

Paper A

Calculation of the Performance of Communication Systems from Measured Oscillator Phase Noise

M. Reza Khanzadi, Dan Kuylenstierna, Ashkan Panahi, Thomas Eriksson, and Herbert Zirath

Accepted for publication in
IEEE Transactions on Circuits and Systems I, Regular Papers
Aug. 2013

Abstract

Oscillator phase noise (PN) is one of the major problems that affect the performance of communication systems. In this paper, a direct connection between oscillator measurements, in terms of measured single-side band PN spectrum, and the optimal communication system performance, in terms of the resulting error vector magnitude (EVM) due to PN, is mathematically derived and analyzed. First, a statistical model of the PN, considering the effect of white and colored noise sources, is derived. Then, we utilize this model to derive the modified Bayesian Cramér-Rao bound on PN estimation, and use it to find an EVM bound for the system performance. Based on our analysis, it is found that the influence from different noise regions strongly depends on the communication bandwidth, i.e., the symbol rate. For high symbol rate communication systems, cumulative PN that appears near carrier is of relatively low importance compared to the white PN far from carrier. Our results also show that $1/f^3$ noise is more predictable compared to $1/f^2$ noise and in a fair comparison it affects the performance less.

Keywords: Phase Noise, Voltage-controlled Oscillator, Phase-Locked Loop, Colored Phase Noise, Communication System Performance, Bayesian Cramér-Rao Bound, Error Vector Magnitude.

1 Introduction

Oscillators are one of the main building blocks in communication systems. Their role is to create a stable reference signal for frequency and timing synchronizations. Unfortunately, any real oscillator suffers from phase noise (PN) which under certain circumstances may be the factor limiting system performance.

In the last decades, plenty of research has been conducted on better understanding the effects of PN in communication systems [1–29]. The fundamental effect of PN is a random rotation of the received signal constellation that may result in detection errors [5, 10]. PN also destroys the orthogonality of the subcarriers in orthogonal frequency division multiplexing (OFDM) systems, and degrades the performance by producing intercarrier interference [3, 6, 8, 12, 17]. Moreover, the capacity and performance of multiple-input multiple-output (MIMO) systems may be severely degraded due to PN in the local oscillators [13, 18, 23, 24]. Further, performance of systems with high carrier frequencies e.g., E-band (60-80 GHz) is more severely impacted by PN than narrowband systems, mainly due to the poor PN performance of high-frequency oscillators [11, 21].

To handle the effects of PN, most communication systems include a *phase tracker*, to track and remove the PN. Performance of PN estimators/trackers is investigated in [5,9,30]. In [31,32], the performance of a PN-affected communication system is computed in terms of error vector magnitude (EVM) and [16,19,22,26] have considered symbol error probability as the performance criterion to be improved in the presence of PN. However, in the communication society, effects of PN are normally studied using quite simple models, e.g, the Wiener process [16, 22, 23, 26–29, 33, 34]. A true Wiener process does not take into account colored (correlated) noise sources [35] and cannot describe frequency and time-domain properties of PN properly [34, 36, 37]. This shows the necessity to employ more realistic PN models in study and design of communication systems.

Finding the ultimate performance of PN-affected communication systems as a function of oscillator PN measurements is highly valuable for designers of communication systems when the goal is to optimize system performance with respect to cost and performance constraints. From the other perspective, a direct relation between PN figures and system performance is of a great value for the oscillator designer in order to design the oscillator so it performs best in its target application.

In order to evaluate the performance of PN-affected communication systems accurately, models that precisely capture the characteristics of non-ideal oscillators are required. PN modeling has been investigated extensively in the circuits and systems community over the past decades [33, 35, 38–48]. The authors in [38, 42, 48] have developed models for the PN based on frequency measurements, where the spectrum is divided into a set of regions with white (uncorrelated) and colored (correlated) noise sources. Similar models have been employed in [33, 46] to derive some statistical properties of PN in time domain.

Among microwave circuit designers, spectral measurements, e.g., single-side band (SSB) PN spectrum is the common figure for characterization of oscillators. Normally SSB PN is plotted versus offset frequency, and the performance is generally benchmarked at specific offset frequencies, e.g., 100 kHz or 1 MHz [11, 49, 50]. In this perspective, oscillators with lower content of colored noise come better out in the comparison, especially when benchmarking for offset frequencies close to the carrier [49].

In this paper, we employ a realistic PN model taking into account the effect of white and colored noise sources, and utilize this model to study a typical point to point communication system in the presence of PN. Note that this is different from the majority of the prior studies (e.g., [16, 22, 23, 26–29, 33, 34]), where PN is modeled as the Wiener process, which is a correct model for oscillators with only white PN sources. Before using the PN model, it is calibrated to fit SSB PN measurements of real oscillators. After assuring that the model describes statistical properties of measured PN over the communication bandwidth, an EVM bound for the system performance is calculated. This is the first time that a direct connection between oscillator measurements, in terms of measured oscillator spectrum, and the optimal communication system performance, in terms of EVM, is mathematically derived and analyzed. Comparing this bound for different PN spectra gives insight into how real oscillators perform in a communication system as well as guidelines to improve the design of oscillators.

The organization and contribution of this paper are as follow:

- In Sec. 2, we first introduce our PN model. Thereafter, the system model of the considered communication system is introduced.

- In Sec. 3, we find the performance of the PN affected communication system in terms of EVM. To do so, we first drive the modified Bayesian Cramér-Rao bound (MBCRB) on the mean square error of the PN estimation. Note that this is the first time that such a bound is obtained for estimation of PN with both white and colored sources. The required PN statistics for calculation of the bound are identified. Finally, the mathematical relation between the MBCRB and EVM is computed.

- In Sec. 4 we derive the closed-from autocorrelation function of the PN increments that is required for calculation of the MBCRB. In prior studies (e.g., [33,39,46]) the focus has been on calculation of the variance of PN increments. However, we show that for calculation of the system performance, the autocorrelation function of the PN increments is the required statistics. The obtained autocorrelation function is valid for free-running oscillators and also the low-order phase-locked loops (PLLs).

- Sec. 5 is dedicated to the numerical simulations. First, the PN sample generation for a given SSB phase spectrum measurement is discussed in brief. Later, the generated samples are used in a Monte-Carlo simulation to evaluate the accuracy of the proposed EVM bound in a practical scenario. Then, we study how the EVM bound is affected by different parts of the PN spectrum. To materialize our theoretical results, the proposed EVM is computed for actual measurements and observations are analyzed. Finally, Sec. 6 concludes the paper.

2 System Model

In this section, we first introduce our PN model in continuous-time domain. Then we present the system model of the considered communication system.

Table 1: Notations

scalar variable	x
vector	$\mathbf{x}$
matrix	$\mathbf{X}$
$(a,b)^{th}$ entry of matrix	$[\cdot]_{a,b}$
continuous-time signal	$x(t)$
discrete-time signal	$x[n]$
statistical expectation	$\mathbb{E}[\cdot]$
real part of complex values	$\Re(\cdot)$
imaginary part of complex values	$\Im(\cdot)$
angle of complex values	$\arg(\cdot)$
natural logarithm	$\log(\cdot)$
conjugate of complex values	$(\cdot)^*$
vector or matrix transpose	$(\cdot)^T$
probability density function (pdf)	$f(\cdot)$
Normal distribution with mean μ and variance σ^2	$\mathcal{N}(x;\mu,\sigma^2)$
second derivative with respect to vector $\mathbf{x}$	$\nabla^2_{\mathbf{x}}$

2.1 Phase Noise Model

In time domain, the output of a sinusoidal oscillator with normalized amplitude can be expressed as

$$V(t) = (1 + a(t))\cos\left(2\pi f_0 t + \phi(t)\right), \tag{1}$$

where f_0 is the oscillator's central frequency, $a(t)$ is the amplitude noise and $\phi(t)$ denotes the PN [41]. The amplitude noise and PN are modeled as two independent random processes. According to [41, 44] the amplitude noise has insignificant effect on the output signal of the oscillator. Thus, hereinafter in this paper, the effect of amplitude noise is neglected and the focus is on the study of the PN process.

In frequency domain, PN is most often characterized in terms of single-side-band (SSB) PN spectrum [33, 41], defined as

$$\mathcal{L}(f) = \frac{P(f_0 + f)}{P_{\text{Total}}}, \tag{2}$$

where $P(f_0 + f)$ is the oscillator power within 1 Hz bandwidth around offset frequency f from the central frequency f_0, and P_{Total} is the total power of the oscillator. For an ideal oscillator where the whole power is concentrated at the central frequency, $\mathcal{L}(f)$ would be

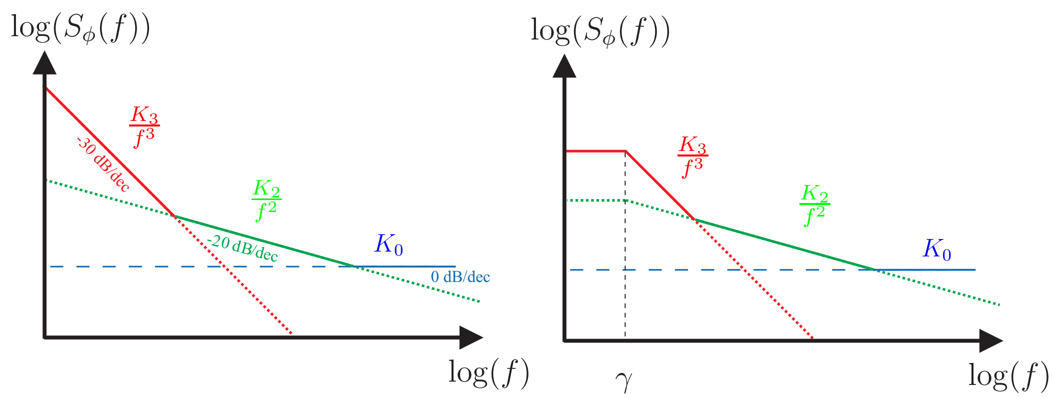

(a) (b)

Figure 1: Phase noise PSD of a typical oscillator. (a) shows the PSD of a free running oscillator. (b) is a model for the PSD of a locked oscillator, where γ is the PLL loop's bandwidth. It is considered that the PN of the reference oscillator is negligible compared to PN of the free running oscillator.

a Dirac delta function at $f = 0$, while, in reality, PN results in spreading the power over frequencies around f_0. It is possible to show that at high frequency offsets, i.e., far from the central frequency, where the amount of PN is small, the power spectral density (PSD) of PN is well approximated with $\mathcal{L}(f)$ found from measurements [33, 43, 48],

$$\mathcal{L}(f) \approx S_\phi(f) \text{ for large } f. \tag{3}$$

The offset frequency range where this approximation is valid depends on the PN performance of the studied oscillator [51]. It can be shown that the final system performance is not sensitive to low frequency events. Thus, for low frequency offsets, we model $S_\phi(f)$ in such a way that it follows the same slope as of higher frequency offsets. In experimental data from free running oscillators, $\mathcal{L}(f)$ normally follows slopes of -30 dB/decade and -20 dB/decade, until a flat noise floor is reached at higher frequency offsets.

According to Demir's model [33], oscillator PN originates from the white and colored noise sources inside the oscillator circuitry. We follow the same methodology and model PN as a superposition of three independent processes

$$\phi(t) = \phi_3(t) + \phi_2(t) + \phi_0(t), \tag{4}$$

where $\phi_3(t)$ and $\phi_2(t)$ model PN with -30 and -20 dB/decade slopes that originate from integration of flicker noise $(1/f)$ (colored noise) and white noise, denoted as $\Phi_3(t)$ and $\Phi_2(t)$, respectively. Further, $\phi_0(t)$ models the flat noise floor, also known as white PN, at higher offset frequencies, that originates from thermal noise and directly results in phase perturbations. In logarithmic scale, the PSD of $\phi_3(t)$, $\phi_2(t)$, and $\phi_0(t)$ can be represented as power-law spectrums [48]:

$$S_{\phi_3}(f) = \frac{K_3}{f^3}, \quad S_{\phi_2}(f) = \frac{K_2}{f^2}, \quad S_{\phi_0}(f) = K_0, \tag{5}$$

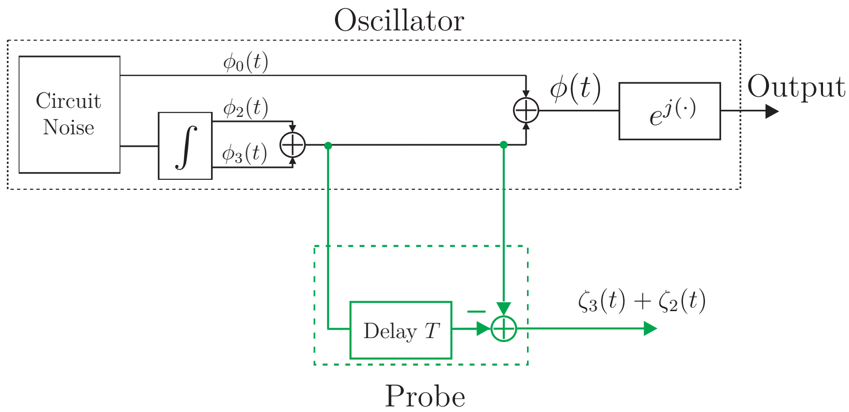

Figure 2: Oscillator's internal phase noise generation model.

where K_3, K_2 and K_0 are the PN levels that can be found from the measurements (see Fig. 1-a).

In many practical systems, the free running oscillator is stabilized by means of a phase-locked loop (PLL). A PLL architecture that is widely used in frequency synchronization consists of a free running oscillator, a reference oscillator, a loop filter, phase-frequency detectors and frequency dividers [33, 52–54]. Any of these components may contribute to the output PN of the PLL. However, PN of the free-running oscillator usually has a dominant effect [52]. A PLL behaves as a high-pass filter for the free running-oscillator's PN, which attenuates the oscillator's PN below a certain cut-off frequency. As illustrated in Fig 1-b, above a certain frequency, PSD of the PLL output is identical to the PN PSD of the free-running oscillator, while below this frequency it approaches a constant value [33, 52–54].

Due to the integration, $\phi_3(t)$ and $\phi_2(t)$ have an *cumulative* nature [33, 48]. PN accumulation over the time delay T can be modeled as the increment phase process

$$\zeta_2(t,T) = \phi_2(t) - \phi_2(t-T) = \int_{t-T}^{t} \Phi_2(\tau)\mathrm{d}\tau, \tag{6a}$$

$$\zeta_3(t,T) = \phi_3(t) - \phi_3(t-T) = \int_{t-T}^{t} \Phi_3(\tau)\mathrm{d}\tau, \tag{6b}$$

that has been called self-referenced PN [52], or the differential PN process [55] in the literature and it is shown that this process can be accurately modeled as a zero-mean Gaussian process (Fig. 2).

2.2 Communication System Model

Consider a single carrier communication system. The transmitted signal $x(t)$ is

$$x(t) = \sum_{n=1}^{N} s[n]p(t-nT), \tag{7}$$

where $s[n]$ denotes the modulated symbol from constellation $\mathcal{C}$ with average symbol energy of E_s, n is the transmitted symbol index, $p(t)$ is a bandlimited square-root Nyquist shaping pulse function with unit-energy, and T is the symbol duration [56]. The continuous-time

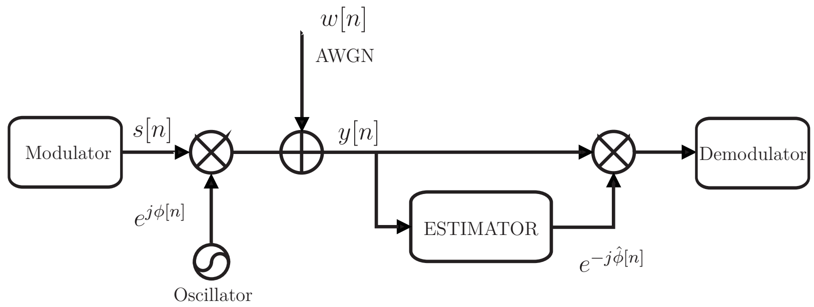

Figure 3: Communication system model with a feedforward carrier phase synchronizer [5].

complex-valued baseband received signal after down-conversion, affected by the oscillator PN, can be written as

$$r(t) = x(t)e^{j\phi(t)} + \tilde{w}(t), \tag{8}$$

where $\phi(t)$ is the oscillator PN modeled in Sec. 2.1 and $\tilde{w}(t)$ is zero-mean circularly symmetric complex-valued additive white Gaussian noise (AWGN), that models the effect of noise from other components of the system. The received signal (8) is passed through a matched filter $p^*(-t)$ and the output is

$$\begin{aligned} y(t) = \int_{-\infty}^{\infty} \sum_{n=1}^{N} s[n]p(t - nT - \tau)p^*(-\tau)e^{j\phi(t-\tau)}\mathrm{d}\tau \\ + \int_{-\infty}^{\infty} \tilde{w}(t-\tau)p^*(-\tau)\mathrm{d}\tau. \end{aligned} \tag{9}$$

Assuming PN does not change over the symbol duration, but changes from one symbol to another so that no intersymbol interference arises[1], sampling the matched filter output (9) at nT time instances results in

$$y(nT) = s[n]e^{j\phi(nT)} + w(nT), \tag{10}$$

that with a change in notation we have

$$y[n] = s[n]e^{j\phi[n]} + w[n], \tag{11}$$

where $\phi[n]$ represents the PN of the n^{th} received symbol in digital domain that is bandlimitted after the matched filter, and $w[n]$ is the filtered (bandlimitted) and sampled version of $\tilde{w}(t)$ that is a zero-mean circularly symmetric complex-valued AWGN with variance σ_w^2. Note that in this work our focus is on oscillator phase synchronization and other synchronization issues, such as time synchronization, are assumed perfect.

[1] The discrete Wiener PN model, which is well studied in the literature is motivated by this assumption (e.g., [5–10, 12, 16, 17, 19, 22–26]). We also refer the reader to the recent studies of this model where the PN variations over the symbol period has also been taken into consideration, and the loss due to the slowly varying PN approximation has been investigated [27–29].

3 System Performance

In this section, we find the performance of the introduced communication system from the PN spectrum measurements. Our final result is in terms of error vector magnitude (EVM), which is a commonly used metric for quantifying the accuracy of the received signal [57,58]. As shown in Fig. 3, PN is estimated at the receiver by passing the received signal through a PN estimator. The estimated PN, denoted as $\hat{\phi}[n]$, is used to de-rotate the received signal before demodulation. The final EVM depends on the accuracy of the PN estimation. In the sequel, we present a bound on the performance of PN estimation, based on the statistics of the PN.

3.1 Background: Cramér-Rao bounds

In order to assess the estimation performance, Cramér-Rao bounds (CRBs) can be utilized to give a lower bound on mean square error (MSE) of estimation [59]. In case of random parameter estimation, e.g., PN estimation, the Bayesian Cramér-Rao bound (BCRB) gives a tight lower bound on the MSE [60]. Consider a burst-transmission system, where a sequence of N symbols $\mathbf{s} = [s[1], \ldots, s[N]]^T$ is transmitted in each burst. According to our system model (11), a frame of signals $\mathbf{y} = [y[1], \ldots, y[N]]^T$ is received at the receiver with the phase distorted by a vector of oscillator PN denoted as $\boldsymbol{\varphi} = [\phi[1], \ldots, \phi[N]]^T$, with the probability density function $f(\boldsymbol{\varphi})$. The BCRB satisfies the following inequality over the MSE of PN estimation:

$$\begin{aligned} &\mathbb{E}_{\mathbf{y},\boldsymbol{\varphi}}\left[(\hat{\boldsymbol{\varphi}} - \boldsymbol{\varphi})(\hat{\boldsymbol{\varphi}} - \boldsymbol{\varphi})^T\right] \geq \mathbf{B}^{-1}, \\ &\mathbf{B} = \mathbb{E}_{\boldsymbol{\varphi}}\left[\mathbf{F}(\boldsymbol{\varphi})\right] + \mathbb{E}_{\boldsymbol{\varphi}}\left[-\nabla^2_{\boldsymbol{\varphi}} \log f(\boldsymbol{\varphi})\right], \end{aligned} \tag{12}$$

where $\hat{\boldsymbol{\varphi}}$ denotes an estimator of $\boldsymbol{\varphi}$, $\mathbf{B}$ is the Bayesian information matrix (BIM) and "$\geq$" should be interpreted as meaning that $\mathbb{E}_{\mathbf{y},\boldsymbol{\varphi}}\left[(\hat{\boldsymbol{\varphi}} - \boldsymbol{\varphi})(\hat{\boldsymbol{\varphi}} - \boldsymbol{\varphi})^T\right] - \mathbf{B}^{-1}$ is positive semi-definite. Here, $\mathbf{F}(\boldsymbol{\varphi})$ is defined as

$$\mathbf{F}(\boldsymbol{\varphi}) = \mathbb{E}_{\mathbf{s}}\left[\mathbb{E}_{\mathbf{y}|\boldsymbol{\varphi},\mathbf{s}}\left[-\nabla^2_{\boldsymbol{\varphi}} \log f(\mathbf{y}|\boldsymbol{\varphi}, \mathbf{s})\right]\right], \tag{13}$$

and it is called modified Fisher information matrix (FIM) in the literature, and bound calculated from (12) is equivalently called the modified Bayesian Cramér-Rao bound (MBCRB) [61]. Based on the definition of the bound in (12), the diagonal elements of $\mathbf{B}^{-1}$ bound the variance of estimation error of the elements of vector $\boldsymbol{\varphi}$

$$\sigma^2_{\varepsilon}[n] \triangleq \mathbb{E}\left[(\underbrace{\phi[n] - \hat{\phi}[n]}_{\triangleq \varepsilon[n]})^2\right] \geq \left[\mathbf{B}^{-1}\right]_{n,n}. \tag{14}$$

From (12)-(14), we note that the estimation error variance is entirely determined by the prior probability density function (pdf) of the PN $f(\boldsymbol{\varphi})$ and the conditional pdf of the received signal $\mathbf{y}$ given the PN and transmitted signal $f(\mathbf{y}|\boldsymbol{\varphi}, \mathbf{s})$ (usually denoted as the likelihood of $\boldsymbol{\varphi}$). In the following, we derive those pdfs based on our models in Sec. 2 and use them in our calculations.

3.2 Calculation of the bound

Calculation of $\mathbb{E}_{\boldsymbol{\varphi}}\left[-\nabla^2_{\boldsymbol{\varphi}} \log f(\boldsymbol{\varphi})\right]$

Based on our PN model (4) and the phase increment process defined in (6), the sampled PN after the matched filter can be written as

$$\begin{aligned}\phi[n] &= \phi_3[n] + \phi_2[n] + \phi_0[n] \\ &= \phi_3[1] + \sum_{i=2}^{n} \zeta_3[i] + \phi_2[1] + \sum_{i=2}^{n} \zeta_2[i] + \phi_0[n],\end{aligned} \tag{15}$$

where $\zeta_3[n] \triangleq \zeta_3(nT,T)$ and $\zeta_2[n] \triangleq \zeta_2(nT,T)$ are the discrete-time phase increment processes, and $\phi_3[1]$ and $\phi_2[1]$ are the cumulative PN of the first symbol in the block, which are modeled as zero-mean Gaussian random variables with a high variance[2], denoted as $\sigma^2_{\phi_3[1]}$ and $\sigma^2_{\phi_2[1]}$, respectively. According to (15) and due to the fact that $\zeta_3[n]$ and $\zeta_2[n]$ are samples from zero-mean Gaussian random processes, $\boldsymbol{\varphi}$ has a zero-mean multivariate Gaussian prior $f(\boldsymbol{\varphi}) = \mathcal{N}(\boldsymbol{\varphi}; \mathbf{0}, \mathbf{C})$, where $\mathbf{C}$ denotes the covariance matrix whose elements are computed in Appendix A as

$$\begin{aligned}[\mathbf{C}]_{l,k} = &\underbrace{\sigma^2_{\phi_3[1]} + \sum_{m=2}^{l} \sum_{m'=2}^{k} R_{\zeta_3}[m-m']}_{\text{from } \phi_3[n]} \\ &+ \underbrace{\sigma^2_{\phi_2[1]} + \sum_{m=2}^{l} \sum_{m'=2}^{k} R_{\zeta_2}[m-m']}_{\text{from } \phi_2[n]} \\ &+ \underbrace{\delta[l-k]\sigma^2_{\phi_0}}_{\text{from } \phi_0[n]}, \\ l,k = &\{1 \dots N\},\end{aligned} \tag{16}$$

where $R_{\zeta_3}[m]$ and $R_{\zeta_2}[m]$ are the autocorrelation functions of $\zeta_3[n]$ and $\zeta_2[n]$, and $\sigma^2_{\phi_0}$ is the variance of $\phi_0[n]$. The required statistics, i.e., $R_{\zeta_3}[m]$, $R_{\zeta_2}[m]$ and $\sigma^2_{\phi_0}$ can be computed from the oscillator PN measurements. To keep the flow of this section, we derive these statistics in Sec. 4, where the final results are presented in (31), (38), (39) and (42). Finally, based on the definition of $f(\boldsymbol{\varphi})$, it is straightforward to show that $\nabla^2_{\boldsymbol{\varphi}} \log f(\boldsymbol{\varphi}) = -\mathbf{C}^{-1}$, and consequently due to the independence of $\mathbf{C}$ from $\boldsymbol{\varphi}$

$$\mathbb{E}_{\boldsymbol{\varphi}}\left[-\nabla^2_{\boldsymbol{\varphi}} \log f(\boldsymbol{\varphi})\right] = \mathbf{C}^{-1}. \tag{17}$$

Calculation of $\mathbb{E}_{\boldsymbol{\varphi}}\left[\mathbf{F}(\boldsymbol{\varphi})\right]$

According to the system model in (11), the likelihood function is written as

$$\begin{aligned}f(\mathbf{y}|\boldsymbol{\varphi}, \mathbf{s}) &= \prod_{n=1}^{N} f\left(y[n]|\phi[n], s[n]\right) \\ &= \left(\frac{1}{\sigma_w^2 \pi}\right)^N \prod_{n=1}^{N} e^{-\frac{|y[n]|^2 + |s[n]|^2}{\sigma_w^2}} \times e^{\frac{2}{\sigma_w^2}\Re\{y[n]s^*[n]e^{-j\phi[n]}\}},\end{aligned} \tag{18}$$

[2]We consider a flat non-informative prior [30, 59] for the initial PN values. To simplify the derivations, it is modeled by a Gaussian distribution with a high variance that is wrapped to a flat prior over $[0, 2\pi]$.

where the first equality is due to independence of the AWGN samples. We can easily show that $\nabla^2_{\boldsymbol{\varphi}} \log f(\mathbf{y}|\boldsymbol{\varphi}, \mathbf{s})$ is a diagonal matrix where its diagonal elements are

$$\begin{aligned}\left[\nabla^2_{\boldsymbol{\varphi}} \log f(\mathbf{y}|\boldsymbol{\varphi}, \mathbf{s})\right]_{n,n} &= \frac{\partial^2 \log f(y[n]|\phi[n], s[n])}{\partial \phi^2[n]} \\ &= -\frac{2}{\sigma_w^2}\Re\{y[n]s^*[n]e^{-j\phi[n]}\}.\end{aligned} \tag{19}$$

Following (13) and (19), diagonal elements of FIM are computed as

$$[\mathbf{F}(\boldsymbol{\varphi})]_{n,n} = \frac{2E_s}{\sigma_w^2}, \tag{20}$$

where E_s is the average energy of the signal constellation. This implies that

$$\mathbf{F}(\boldsymbol{\varphi}) = \frac{2E_s}{\sigma_w^2}\mathbf{I}, \tag{21}$$

where $\mathbf{I}$ is the identity matrix. Finally, from (12), (17), and (21)

$$\mathbf{B} = \frac{2E_s}{\sigma_w^2}\mathbf{I} + \mathbf{C}^{-1}. \tag{22}$$

The minimum MSE of PN estimation (14) depends on SSB PN spectrum measurements through $\mathbf{B}$ and $\mathbf{C}^{-1}$. We will use this result in the following subsection to calculate a more practical performance measure that is called EVM.

3.3 Calculation of Error Vector Magnitude

The modulation accuracy can be quantified by the EVM, defined as the root-mean square error between the transmitted and received symbols [57, 58]

$$\mathrm{EVM}[n] = \sqrt{\frac{\frac{1}{M}\sum_{k=1}^{M}|s_k[n] - s'_k[n]|^2}{E_s}}, \tag{23}$$

where $s_k[n]$, $k \in \{1, \ldots, M\}$, is the transmitted symbol from the constellation $\mathcal{C}$ with order M, at the n^{th} time instance, and $s'_k[n]$ is the distorted signal at the receiver. Even with optimal PN estimators, we have residual phase errors. Hence, cancellation of PN by de-rotation of the received signal with the estimated PN results in a distorted signal

$$\begin{aligned}s'_k[n] &= s_k[n]e^{j(\phi[n]-\hat{\phi}[n])} \\ &= s_k[n]e^{j\varepsilon[n]},\end{aligned} \tag{24}$$

where $\varepsilon[n]$ is the residual phase error. Before going further, assume we have used an PN estimator [59] that reaches the computed MBCRB, and estimation error $\varepsilon[n]$ is a zero-mean Gaussian random variable. Our numerical evaluations in the result section support the existence of such estimators (Fig. 6). This implies that $f(\varepsilon[n]) = \mathcal{N}(\varepsilon[n]; 0, \sigma_\varepsilon^2[n])$, where $\sigma_\varepsilon^2[n]$ is defined in (14) and can be computed from the derived MBCRB. The variance obtained from the MBCRB results from averaging over all possible transmitted symbols. Note that to calculate the EVM accurately, we need to use the conditional PDF of the residual PN variance $f(\varepsilon[n]|\mathbf{s})$. However, in order to keep our analysis less complex we approximate the conditional PDF with the unconditional one: $f(\varepsilon[n]|\mathbf{s}) \approx f(\varepsilon[n])$. Our numerical simulations show the validity of this approximation in several scenarios of interest (Fig. 7). For the sake of notational simplicity, we drop the time index n in the following calculations. Averaging over all possible values of $\varepsilon[n]$, (23) is rewritten as

$$\mathrm{EVM}[n] = \sqrt{\frac{\frac{1}{M}\sum_{k=1}^{M}\mathbb{E}_{\varepsilon}\Big[|s_k - s_k e^{j\varepsilon}|^2\Big]}{E_s}}. \tag{25}$$

The magnitude square of the error vector for a given $\varepsilon[n]$, and $s_k[n]$ is determined as

$$\begin{aligned}|s_k - s_k e^{j\varepsilon}|^2 &= 2|s_k|^2(1-\cos(\varepsilon))\\ &= 4|s_k|^2\sin^2(\frac{\varepsilon}{2}),\end{aligned} \tag{26}$$

and consequently

$$\frac{1}{M}\sum_{k=1}^{M}\mathbb{E}_{\varepsilon}\Big[|s_k - s_k e^{j\varepsilon}|^2\Big] = 4\frac{1}{M}\sum_{k=1}^{M}|s_k|^2\mathbb{E}_{\varepsilon}\Big[\sin^2(\frac{\varepsilon}{2})\Big]. \tag{27}$$

The expectation in (27) can be computed as

$$\begin{aligned}\mathbb{E}_{\varepsilon}\Big[\sin^2(\frac{\varepsilon}{2})\Big] &= \int_{-\infty}^{\infty}\sin^2(\frac{\varepsilon}{2})f(\varepsilon)\mathrm{d}\varepsilon\\ &= (1-e^{-\sigma_{\varepsilon}^2/2})/2,\end{aligned} \tag{28}$$

where $f(\varepsilon)$ is the Gaussian pdf of $\varepsilon[n]$ as defined before.

Finally, EVM can be computed from (25), (27), and (28) as

$$\begin{aligned}\mathrm{EVM}[n] &= \sqrt{2(1-e^{-\sigma_{\varepsilon}^2[n]/2})}\\ &= \sqrt{2(1-\exp\left([-0.5\mathbf{B}^{-1}]_{n,n}\right)}\\ &= \sqrt{2-2\exp\left(-0.5\left[\left(\frac{2E_s}{\sigma_w^2}\mathbf{I}+\mathbf{C}^{-1}\right)^{-1}\right]_{n,n}\right)},\end{aligned} \tag{29}$$

where $\mathbf{C}$ is calculated in (16) and it is a function of PN model parameters K_3, K_2, and K_0 through $R_{\zeta_3}[m]$, $R_{\zeta_2}[m]$ and $\sigma_{\phi_0}^2$, computed in Sec. 4.

4 Phase Noise Statistics

As we can see in Sec. 3, the final system performance computed in terms of EVM (29) depends on the minimum MSE of the PN estimation defined in (14). According to (16), in order to find the minimum PN variance, we have to compute the required PN statistics; i.e., $R_{\zeta_3}[m]$, $R_{\zeta_2}[m]$ and $\sigma_{\phi_0}^2$. To find these statistics we need to start from our continuous-time PN model described in Sec. 2.1. Based on (6), $\phi_3(t)$ and $\phi_2(t)$ result from integration of noise sources inside the oscillator. On the other hand, $\phi_0(t)$ has external sources. Therefore, we separately study the statistics of these two parts of the PN.

4.1 Calculation of $\sigma^2_{\phi_0}$

The PSD of $\phi_0(t)$ is defined as

$$S_{\phi_0}(f) = K_0, \tag{30}$$

where K_0 is the level of the noise floor that can be found from the measurements, and according to (2), it is normalized with the oscillator power [38]. The system bandwidth is equal to the symbol rate[3] $1/T$, and at the receiver, a low-pass filter with the same bandwidth is applied to the received signal $x(t)e^{j\phi_0(t)}$. According to [62], if K_0/T is small (which is generally the case in practice), low-pass filtering of the received signal results in filtering of $\phi_0(t)$ with the same bandwidth. Therefore we are interested in the part of the PN process inside the system bandwidth. The variance of the bandlimited $\phi_0(t)$ is calculated as

$$\sigma^2_{\phi_0} = \int_{-1/2T}^{+1/2T} S_{\phi_0}(f)\mathrm{d}f = \frac{K_0}{T}. \tag{31}$$

As $\phi_0(t)$ is bandlimited, we can sample it without any aliasing.

4.2 Calculation of $R_{\zeta_3}[m]$ and $R_{\zeta_2}[m]$

It is possible to show that $\zeta_3(t, T)$ and $\zeta_2(t, T)$ defined in (6) are stationary processes and their variance over the time delay T, is proportional to T and T^2, respectively [33, 39, 46]. However, as shown in this work, their variance is not enough to judge the effect of using a noisy oscillator on the performance of a communication system, and hence their autocorrelation functions must be also taken into consideration. Samples of $\zeta_3(t, T)$ and $\zeta_2(t, T)$ can be found by applying a delay-difference operator on $\phi_3(t)$ and $\phi_2(t)$, respectively [33, 46], which is a linear time invariant sampling system with impulse response of

$$h(t) = \delta(t) - \delta(t - T). \tag{32}$$

Starting from $\phi_2(t)$, the PSD of $\zeta_2(t, T)$ can be computed as

$$S_{\zeta_2}(f) = S_{\phi_2}(f)|H(j2\pi f)|^2, \tag{33}$$

where $H(j2\pi f) = 1 - e^{-j2\pi fT}$ is the frequency response of the delay-difference operator introduced in (32). The autocorrelation function of $\zeta_2(t, T)$ can be computed by taking the inverse Fourier transform of its PSD

$$R_{\zeta_2}(\tau) = \int_{-\infty}^{+\infty} S_{\zeta_2}(f)e^{j2\pi f\tau}\mathrm{d}f, \tag{34}$$

where τ is the time lag parameter. Using (33) and (34) the continuous-time auto correlation function can be found as

$$R_{\zeta_2}(\tau) = 8\int_0^{+\infty} S_{\phi_2}(f)\sin(\pi fT)^2\cos(2\pi f\tau)\mathrm{d}f. \tag{35}$$

[3] This bandwidth corresponds to using a raised-cosine pulse shaping filter $p(t)$ defined in (7) with zero excess bandwidth. For the general case, the bandwidth becomes $(1 + \alpha)/T$ where α denotes the excess bandwidth [56].

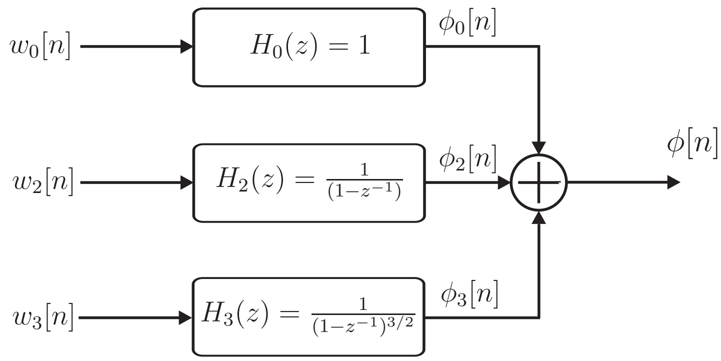

Figure 4: Phase noise sample generator.

As can be seen in (35), in order to find the closed-form autocorrelation functions, we do not confine our calculations inside the system bandwidth $1/T$. However, we see from the measurements that parts of $\phi_3(t)$ and $\phi_2(t)$ outside bandwidth are almost negligible and do not have any significant effect on the calculated autocorrelation functions.

The PSD of $\phi_2(t)$ has the form of

$$S_{\phi_2}(f) = \frac{K_2}{f^2 + \gamma^2}, \tag{36}$$

where K_2 and can be found from the measurements and γ is a low cut-off frequency that is considered to be very small for a free running oscillator, while it is set to the PLL's loop bandwidth in case of using a locked oscillator (Fig. 1-b). According to (35) and (36), autocorrelation function of $\zeta_2(t, T)$ can be determined as

$$\begin{aligned} R_{\zeta_2}(\tau) &= 8 \int_0^{+\infty} \frac{K_2}{f^2 + \gamma^2} \sin(\pi f T)^2 \cos(2\pi f \tau) \mathrm{d}f \\ &= \frac{K_2 \pi}{\gamma} \left(2e^{-2\gamma\pi|\tau|} - e^{-2\gamma\pi|\tau - T|} - e^{-2\gamma\pi|\tau + T|} \right). \end{aligned} \tag{37}$$

Sampling (37) results in

$$R_{\zeta_2}[m] = \frac{K_2 \pi}{\gamma} \left(2e^{-2\gamma\pi T|m|} - e^{-2\gamma\pi T|m-1|} - e^{-2\gamma\pi T|m+1|} \right), \tag{38}$$

where $R_{\zeta_2}[m] \triangleq R_{\zeta_2}(mT)$. For a free running oscillator, the autocorrelation function can be found by taking the limit of (38) as γ approaches 0, that results in

$$R_{\zeta_2}[m] = \begin{cases} 4K_2\pi^2 T & \text{if } m = 0 \\ 0 & \text{otherwise} \end{cases}. \tag{39}$$

Results in (38) and (39) show that for a locked oscillator $\zeta_2[n]$ is a colored process (its samples are correlated with each other), while it is white for a free running oscillator. To find $R_{\zeta_3}[m]$ for a free running oscillator, one can consider the PSD of $\phi_3(t)$ to be $S_{\phi_3}(f) \propto 1/f^3$. However, by doing so, $S_{\zeta_3}(f)$ defined in (33) diverges to infinity at zero offset frequency and hence makes it impossible to find the autocorrelation function in this case. To resolve the divergence problem, we follow a similar approach to [33, 46] and introduce a low cutoff frequency γ below which $S_{\phi_3}(f)$ flattens. Our numerical studies show that as long as γ is chosen reasonably small, its value does not have any significant effect on the final result. Similar to our analysis for ϕ_2, the autocorrelation of PN increments at the output of a first order PLL can be found by setting γ equal to the PLL's loop bandwidth. Hence, we define the PSD of $\phi_3(t)$ as

$$S_{\phi_3}(f) = \frac{K_3}{|f|^3 + \gamma^3}, \tag{40}$$

where K_3 can be found from the measurements (Fig. 3). Following the same procedure of calculating $R_{\zeta_2}(\tau)$ in (33-35) and using (40), the autocorrelation function of $\zeta_3(t)$ can be computed by solving the following integral

$$R_{\zeta_3}(\tau) = 8\int_0^{+\infty} \frac{K_3}{f^3 + \gamma^3} \sin(\pi f T)^2 \cos(2\pi f \tau)\mathrm{d}f. \tag{41}$$

This integral is solved in the Appendix B. Finally, the closed-form sampled autocorrelation function of $\zeta_3[n]$ is derived as

$$R_{\zeta_3}[0] = -8K_3\pi^2T^2\left(\Lambda + \log(2\pi\gamma T)\right), \tag{42a}$$

$$R_{\zeta_3}[\pm 1] = -8K_3\pi^2T^2(\Lambda + \log(8\pi\gamma T)), \tag{42b}$$

otherwise

$$\begin{aligned} R_{\zeta_3}[m] = -8K_3\pi^2T^2\Big[& -m^2(\Lambda + \log(2\pi\gamma T|m|)) \\ & + \frac{(m+1)^2}{2}(\Lambda + \log(2\pi\gamma T|m+1|)) \\ & + \frac{(m-1)^2}{2}(\Lambda + \log(2\pi\gamma T|m-1|))\Big], \end{aligned} \tag{42c}$$

where $\Lambda \triangleq \Gamma - 3/2$, and $\Gamma \approx 0.5772$ is the Euler-Mascheroni constant [63]. The calculated variance $R_{\zeta_3}[0]$ is almost proportional to T^2 which is similar to the results of [33, 46]. As it can be seen from (42), samples of $\zeta_3[n]$ are correlated in this case which is in contrast to $\zeta_2[n]$. Consequently, in presence of $\phi_3(t)$, variance of $\zeta_3[n]$ is not adequate to judge the behavior of the oscillator in a system; it is necessary to incorporate the correlation properties of $\zeta_3[n]$ samples.

5 Numerical and Measurement Results

In this section, first the analytical results obtained in the previous sections are evaluated by performing Monte-Carlo simulations. Then, the proposed EVM bound is used to quantify the system performance for a given SSB PN measurement.

5.1 Phase Noise Simulation

To evaluate our proposed EVM bound, we first study the generation of time-domain samples of PN that match a given PN SSB measurement in the frequency domain. As shown in (4), we model PN as a summation of three independent noise processes $\phi_3(t)$,

$\phi_2(t)$, and $\phi_0(t)$. The same model is followed to generate time-domain samples of the total PN process (Fig. 4). Generating the samples of power-law noise with PSD of $1/f^{\alpha}$ has been vastly studied in the literature [34, 64, 65]. One suggested approach in [64] is to pass independent identically distributed (iid) samples of a discrete-time Gaussian noise process through a linear filter with the impulse response of

$$H(z) = \frac{1}{(1 - z^{-1})^{\alpha/2}}. \tag{43}$$

The PSD of the generated noise can be computed as

$$S^d(f) = \sigma^2_{w_\alpha} H(z)H(z^{-1})T, \tag{44}$$

where T is the sampling time equal to the symbol duration, and $\sigma^2_{w_\alpha}$ is the variance of input iid Gaussian noise [64]. Fig. 4 illustrates the block diagram used for generating the total PN process. Tab. 2 shows variance of the input iid Gaussian noise in each branch calculated based on (44).

Table 2: PN generation: Input iid Noise Variance

PN Process	PSD	Input Noise Variance
$\phi_0[n]$	K_0	$\sigma^2_{w_0} = K_0/T$
$\phi_2[n]$	K_2/f^2	$\sigma^2_{w_2} = 4K_2T\pi^2$
$\phi_3[n]$	K_3/f^3	$\sigma^2_{w_3} = 8K_3T^2\pi^3$

Fig. 5 shows the total one-sided PSD of the generated PN samples for a particular example. The frequency figures of merits are set to be $K_0 = -110$ dB, $K_3 = 10^4$, and $K_2 = 10$. According to Tab. 2, the variance of input white Gaussian noises to the PN generation system in Fig. 4 for a system with symbol rate 10^6 symbol/sec are calculated to be $\sigma^2_{w_0} = 5 \times 10^{-6}$, $\sigma^2_{w_2} = 1.97 \times 10^{-4}$, and $\sigma^2_{w_3} = 1.26 \times 10^{-6}$. This figure shows that generated time-domain samples match to the PSD of PN.

5.2 Monte-Carlo Simulation

Consider a communication system like that of Fig. 3. Two modulation schemes i.e., 16-QAM and 64-QAM are used and length of the communication block is set to 200 symbols. A local oscillator with the PN PSD of Fig. 5 is used. For the Monte-Carlo simulation, we first generate the PN samples following the routine proposed in Sec. 5.1. Then, we design the maximum a posteriori (MAP) estimator of the PN vector $\boldsymbol{\varphi}$ at the receiver. The MAP estimator is a Bayesian estimator that can be used for estimation of random parameters [59, 60]. This estimator finds $\hat{\boldsymbol{\varphi}}$ that maximizes the posteriori distribution of $\boldsymbol{\varphi}$:

$$\begin{aligned} \hat{\boldsymbol{\varphi}}_{\mathrm{MAP}} &= \arg\max_{\boldsymbol{\varphi}} \; f(\boldsymbol{\varphi}|\mathbf{y}, \mathbf{s}) \\ &= \arg\max_{\boldsymbol{\varphi}} \; f(\mathbf{y}|\boldsymbol{\varphi}, \mathbf{s}) f(\boldsymbol{\varphi}). \end{aligned} \tag{45}$$

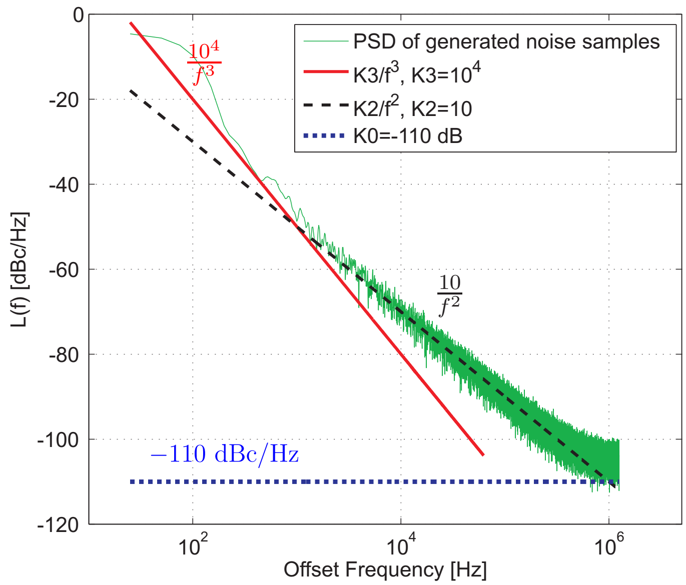

Figure 5: PSD of the generated PN samples vs. the theoretical PSD. The generated phase noise PSD is matched to the desired PSD with the given values of K_0, K_1 and K_3.

The needed likelihood and prior functions for designing this estimator are calculated in Sec. 3. However, the detailed implementation of this estimator is not in the focus of this paper and we focus only on the final results. We refer the interested reader to [9, 59, 60] for more information on implementation of the MAP and other Bayesian estimators such as Kalman or particle filters, that can be used for estimation of random parameters. The estimated phase values from the MAP estimator are used to eliminate the effect of PN by de-rotation of the received signals. Finally, the EVM is computed by comparing the transmitted symbols with the signal after PN compensation. Fig. 6 shows the density of the residual phase errors for two of the symbols in the frame ($n = 2$ and $n = 100$). It can be seen that phase errors are almost zero mean and have Gaussian distribution. PN in the middle of the block can be estimated better has a lower residual variance. Fig. 7 compares the proposed theoretical EVM bound (average EVM over the block) against the resulted EVM calculated from the Monte-Carlo simulation of a practical system. In this simulation, 16-QAM and 64-QAM modulations are used, where 10% of the symbols are known (pilot symbols) at the receiver. For the unknown symbols, decision-feedback from a symbol detector is used at the estimator. It can be seen that the calculated EVM from the empirical simulation matches the proposed theoretical bound at moderate and high SNRs. It can also be seen that at low SNR, the bound is more accurate for 16-QAM modulation format. This is mainly due to the fact that 16-QAM has a lower symbol error probability than 64-QAM for a given SNR, thus the decision-feedback is more accurate in this case.

5.3 Analysis of the Results

Now, when the EVM bound is evaluated, the system performance for a given oscillator spectrum may be quantified. In this section we study how the EVM is affected by white

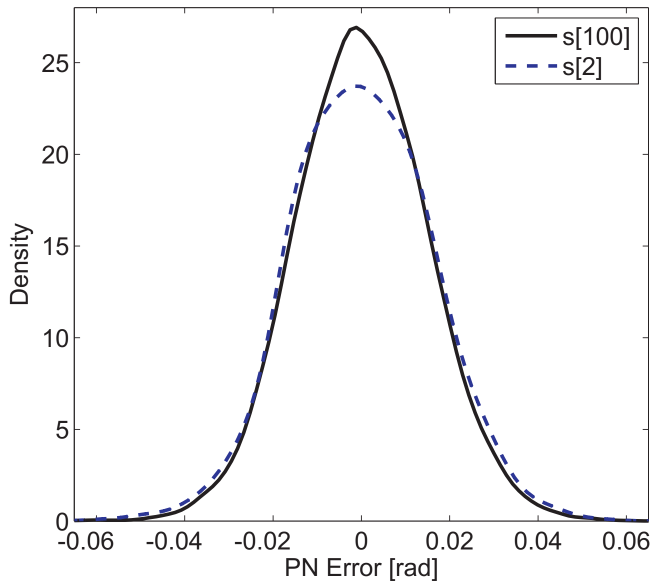

Figure 6: The phase error distribution of the second symbol ($n = 2$) and mid symbol of the block ($n = 100$) estimated from 10000 simulation trials. It can be seen that the phase error distribution is almost zero-mean Gaussian for both symbols. PN of the symbol in the middle of the block can be estimated better and has a lower residual variance.

PN (PN floor) and cumulative PN, respectively. The effect from cumulative PN is further divided into origins from white and colored noise sources, i.e., SSB PN slopes of -30 dB/decade and -20 dB/decade, respectively. It is found that the influence from the different noise regions strongly depends on the communication bandwidth, i.e., the symbol rate. For high symbol rates, white PN is more important compared to the cumulative PN that appears near carrier.

Fig. 8 compares the performance sensitivity of two communication systems with different bandwidths, namely System A and System B against a set of different noise floor levels. System A operates with the symbol rate of 0.1 MSymbols/s that leads to 10 μs symbol duration. In contrast, System B has 5 MSymbols/s symbol rate results in 0.2 μs symbol time that is almost 50 times shorter than that of System A. It is seen in Fig. 8 that an increase in the level of white PN affects the System B with high symbol rate much more than the more narrowband System A system. This result can be intuitively understood, since in a system with a higher symbol rate, symbols are transmitted over a shorter period of time and thus experience smaller amount of cumulative PN. On the other hand, the amount of phase perturbation introduced by the white PN is a function of the system bandwidth and a wideband system integrates a larger amount of white PN (31). Therefore, in contrast to the cumulative PN, white PN affects a system with high bandwidth more compared to a system with a narrower bandwidth.

The next step is to identify the different effects from cumulative PN originating in white noise sources (slope -20 dB/decade) and cumulative PN originating in colored noise sources (slope -30 dB/decade). Fig. 9 shows the effect of changing the corner frequency on the performance of the introduced systems by increasing the level of $1/f^3$ noise, K_3. Other parameters such as K_2 and K_0 are kept constant in this simulation to just

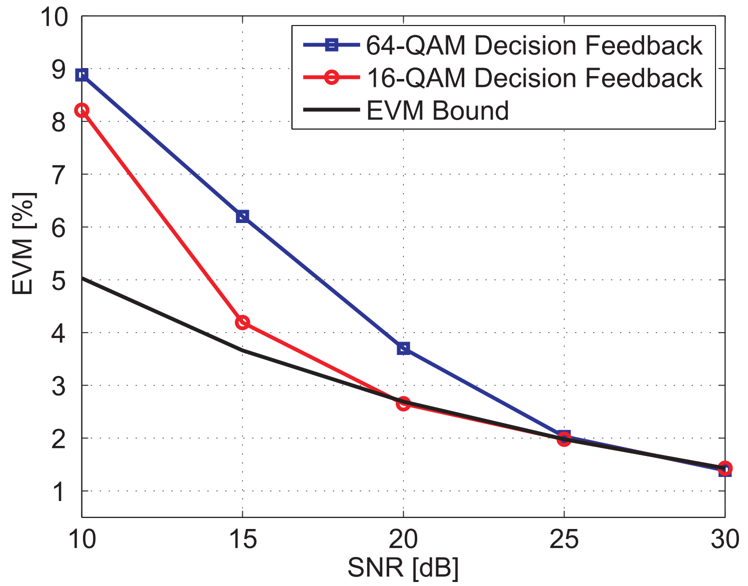

Figure 7: Proposed theoretical EVM bound vs. the EVM from the Monte-Carlo simulation. The PSD in Fig. 5 is considered as the PN PSD. 16 and 64-QAM modulations are used, pilot density is 10%, and the symbol rate is set to 10^6 [Symbol/sec]. Note that in pure AWGN case, the symbol error probability of 16-QAM at SNR= 20 dB is 10^{-5} and for 64-QAM it is 10^{-4} at SNR=25 dB.

capture the effect of different values of K_3. Intuitively the performance degrades when the noise level is increased. However, as seen in Fig. 9, the EVM is not significantly affected below certain corner frequencies ($f_{\text{corner}} < 10$ kHz for System A and $f_{\text{corner}} < 1$ MHz for System B). This constant EVM is due to the dominant effect of $1/f^2$ on the performance. By increasing the corner frequency, after a certain point $1/f^3$ becomes more dominant which results in a continuous increase in EVM. It can also be seen that System A is more sensitive to increase of the $1/f^3$ noise level. Because of the higher bandwidth, System B contains more of the $1/f^2$ noise which is constant and dominates the $1/f^3$ effect, and its EVM stays unchanged for a larger range of corner frequencies.

Fig. 10 illustrates the effect of increasing the low cut-off frequency γ on the EVM bound. As mentioned before, the PN spectrum after a PLL can be modeled similar to a free running oscillator with a flat region below a certain frequency. In our analysis, γ is the low cut-off frequency below which the spectrum flatten. It can be seen that changes of γ below certain frequencies ($\gamma < 1$ kHz) does not have any significant effect on the calculated EVM. However, by increasing γ more, the effect of the flat region becomes significant and the final EVM decreases.

Finally, we compare the individual effect of $1/f^2$ PN and $1/f^3$ PN on the performance. Consider two SSB PN spectrums as illustrated in Fig. 11. One of the spectrums contains pure $1/f^2$ PN while $1/f^3$ PN is dominant in another. In a system with the symbol rate of 3.84 MSymbols/s (bandwidth of 3.84 MHz), the variance of phase increment process for both spectrums is equal to $R_\zeta(\tau = 0) = 6.2 \times 10^{-7}$ [rad^2]. However, comparing the EVM values shows that the spectrum with pure $1/f^3$ PN results in 2.36 dB lower EVM. This is due to the correlated samples of phase increment process for $1/f^3$ noise which results in lower PN estimation errors compared to $1/f^2$ noise.

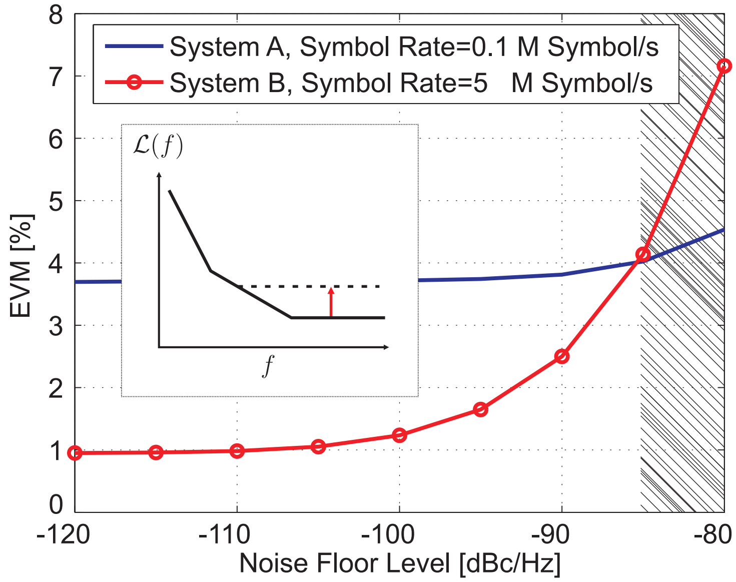

Figure 8: The proposed theoretical EVM bound against different noise floor levels. $K_2 = 1$ and $K_3 = 10^4$ are kept constant. The low cut-off frequency γ is considered to be 1 Hz and SNR= 30 dB and block-length is set to 10. In the hatched regime, the white PN (noise floor) dominates over the cumulative part of the PN.

5.4 Measurements

To materialize the analytical discussion above, Fig. 12 and Fig. 13 show the measured SSB PN spectrums from a GaN HEMT MMIC oscillator under two different bias conditions with drastically different characteristics for the cumulative PN. Fig. 12 shows the spectrum for the oscillator biased at a drain voltage of Vdd = 6 V and drain current of Id = 30 mA. At this bias condition, the $1/f$ noise (flicker noise) from the transistor is fairly low. The corner frequency between the -30 dB/decade and -20 dB/decade regions can be clearly detected at 83.3 kHz. In contrast, Fig. 13 shows a spectrum from the same oscillator biased at Vdd = 30 V and Id = 180 mA. Under this bias condition the noise from colored noise sources is increased significantly and the cumulative PN has -30 dB/decade slope until it reaches the white PN floor. Further, the power of the oscillator is higher in Fig 12, resulting in a lower level for the white PN. Fig. 14 compares EVM for the SSB PN spectrums in Figs. 12 and 13, respectively, versus the symbol rate. As expected based on the results in Sec. 5.3, the spectrum in Fig 12 gives the best EVM for low symbol rates, while the spectrum in Fig 13 gives the best EVM for higher symbol rates as a result of the lower level of white PN.

6 Conclusions

In this paper, a direct connection between oscillator measurements, in terms of measured single-side band PN spectrum, and the optimal communication system performance, in terms of EVM, is mathematically derived and analyzed. First, we found the statistical model of the PN which considers the effect of white and colored noise sources. Then, we utilized this model to derive the modified Bayesian Cramér-Rao bound on PN estimation

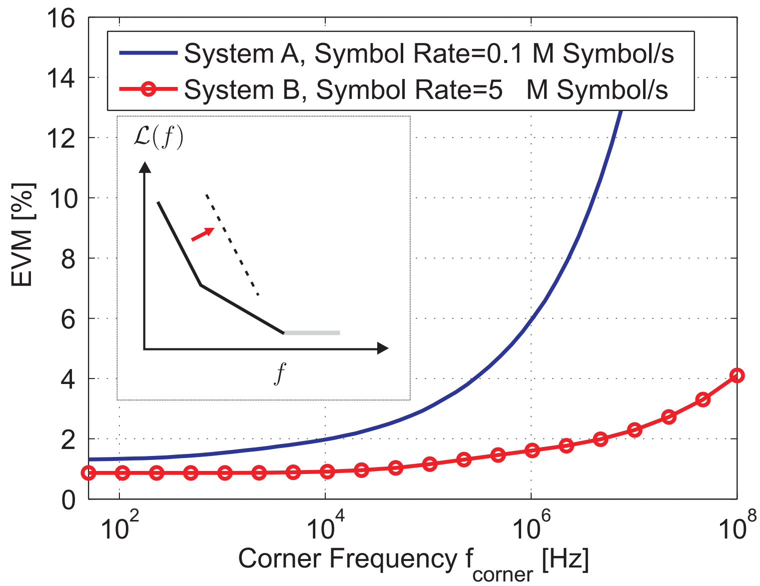

Figure 9: The proposed theoretical EVM bound against different values of corner frequency f_{corner} for two systems with different bandwidth. $K_2 = 0.1$ and $K_0 = -160$ dBc/Hz are kept constant and f_{corner} is increased by adding to K_3. The low cut-off frequency γ is considered to be 1 Hz and SNR= 30 dB and block-length is set to 10.

that is used to find an EVM bound for the system performance.

The paper demonstrates that for high symbol rate communication systems, the near carrier cumulative PN is of relatively low importance compared to white PN far from carrier. Our results also show that $1/f^3$ noise is more predictable compared to $1/f^2$ noise, and in a fair comparison it affects the system performance less. These findings will have important effects on design of hardware for frequency generation as well as the requirements on voltage controlled oscillator design, choice of reference oscillators and loop bandwidth in the phase-locked loops.

Although in several empirical measurements of oscillators $1/f^3$, $1/f^2$, and f^0-shaped noise dominate the PN spectrum, there has been studies where other slopes ($1/f^4$, $1/f^1$) have been observed in the measurements. Our PN model can be extended in future studies to include the effect of various noise statistics. Our current analysis can be used in order to study free running oscillators, and it is valid for study of phase-locked loops up to some extent. Further, our theoretical results can be extended for a more thorough study of phase-locked loops. In our analysis, the transition from continuous to discrete-time domain was based on a slow-varying PN assumption. A more sophisticated study can be conducted to analyze the effect of relaxing this assumption. Finally, we analyzed a single carrier communication system. It is interesting to extend this work to the case of multi-carrier communication systems.

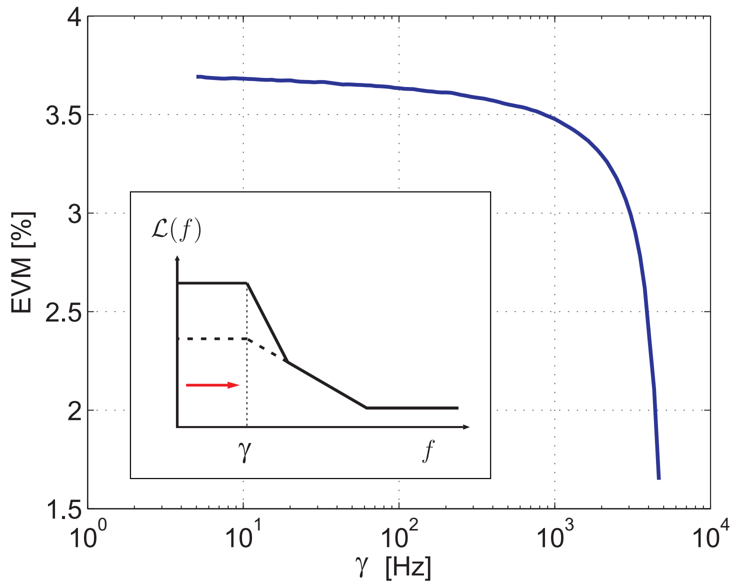

Figure 10: The proposed theoretical EVM bound against different values of low cut-off frequency γ. $K_2 = 10^4$, $K_2 = 1$ and $K_0 = -160$ dBc/Hz are kept constant, SNR= 30 dB and symbol rate is 1 M Symbol/s.

7 Appendix A

In this appendix, elements of the covariance matrix $\mathbf{C}$ are calculated. According to (15), and stationarity of the PN increments

$$
\begin{aligned}
[\mathbf{C}]_{l,k} &= \mathbb{E}\Big[\Big(\phi[l] - \mathbb{E}[\phi[l]]\Big)\Big(\phi[k] - \mathbb{E}[\phi[k]]\Big)\Big] \\
&= \mathbb{E}\Big[\Big(\phi_0[l] + \phi_3[1] + \phi_2[1] + \sum_{m=2}^{l}(\zeta_3[m] + \zeta_2[m])\Big) \\
&\qquad \times \Big(\phi_0[k] + \phi_3[1] + \phi_2[1] + \sum_{m'=2}^{k}(\zeta_3[m'] + \zeta_2[m'])\Big)\Big] \\
&= \mathbb{E}\Big[\phi_3[1]\phi_3[1]\Big] + \mathbb{E}\Big[\phi_2[1]\phi_2[1]\Big] + \mathbb{E}\Big[\phi_0[l]\phi_0[k]\Big] \\
&\qquad + \sum_{m=2}^{l}\sum_{m'=2}^{k}\mathbb{E}\Big[\zeta_3[m]\zeta_3[m']\Big] + \mathbb{E}\Big[\zeta_2[m]\zeta_2[m']\Big] \\
&\qquad + \mathbb{E}\Big[\phi_3[1] \times \sum_{m=2}^{l}\zeta_3[m]\Big] + \mathbb{E}\Big[\phi_3[1] \times \sum_{m'=2}^{k}\zeta_3[m']\Big] \\
&\qquad + \mathbb{E}\Big[\phi_2[1] \times \sum_{m=2}^{l}\zeta_2[m]\Big] + \mathbb{E}\Big[\phi_2[1] \times \sum_{m'=2}^{k}\zeta_2[m']\Big], \qquad l,k = \{1 \ldots N\}. \qquad (46)
\end{aligned}
$$

Note that in calculation of the MBCRB, we need to compute the inverse of the covariance matrix $\mathbf{C}$. It is possible to mathematically show that the correlations between the initial PN of the block and future PN increments (the four last terms in (46)) do not have any effect on $\mathbf{C}^{-1}$. Therefore, we omit those terms in our calculations and finally the

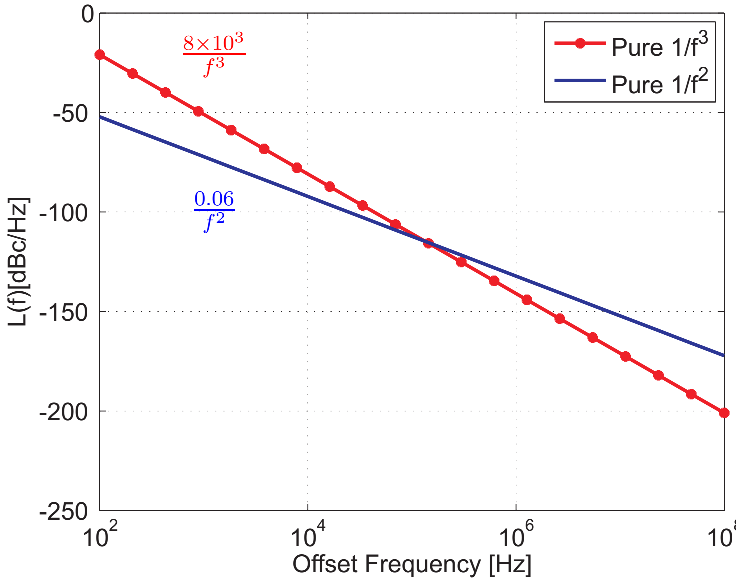

Figure 11: Two SSB PN spectrums with pure $1/f^2$ PN and $1/f^3$ PN. We assume the two spectrums have a very low white PN level. For a system with the symbol rate of 3.84 MSymbols/s, both spectrums result in the same variance of phase increments $R_\zeta(\tau = 0) = 6.2 \times 10^{-7}$ [rad^2].

covariance matrix can be written as

$$\begin{aligned}[\mathbf{C}]_{l,k} =& \sigma^2_{\phi_3[1]} + \sigma^2_{\phi_2[1]} + \delta[l-k]\sigma^2_{\phi_0} \\ &+ \sum_{m=2}^{l}\sum_{m'=2}^{k} R_{\zeta_3}[m-m'] + R_{\zeta_2}[m-m'], \qquad l,k = \{1\ldots N\}. \end{aligned} \tag{47}$$

8 Appendix B

Steps taken to solve the integral in (41) are described here. We can write (41) as

$$\begin{aligned} R_{\zeta_3}(\tau) &= 8\int_0^{+\infty} \frac{K_3}{f^3+\gamma^3}\sin(\pi f T)^2\cos(2\pi f\tau)\mathrm{d}f \\ &= 4\int_0^{+\infty} \frac{K_3}{f^3+\gamma^3}\cos(2\pi f\tau)\mathrm{d}f \\ &\quad - 2\int_0^{+\infty} \frac{K_3}{f^3+\gamma^3}\cos(2\pi f(|\tau+T|)\mathrm{d}f \\ &\quad - 2\int_0^{+\infty} \frac{K_3}{f^3+\gamma^3}\cos(2\pi f(|\tau-T|)\mathrm{d}f. \end{aligned} \tag{48}$$

It is clear that solving the integral in the form of $\int_0^{+\infty} K_3/(f^3+\gamma^3)\cos(2\pi f\tau)\mathrm{d}f$ is enough to compute the total integral of (48). This integral is complicated enough that powerful software such as Mathematica are not able to converge to the final answer. Consequently,

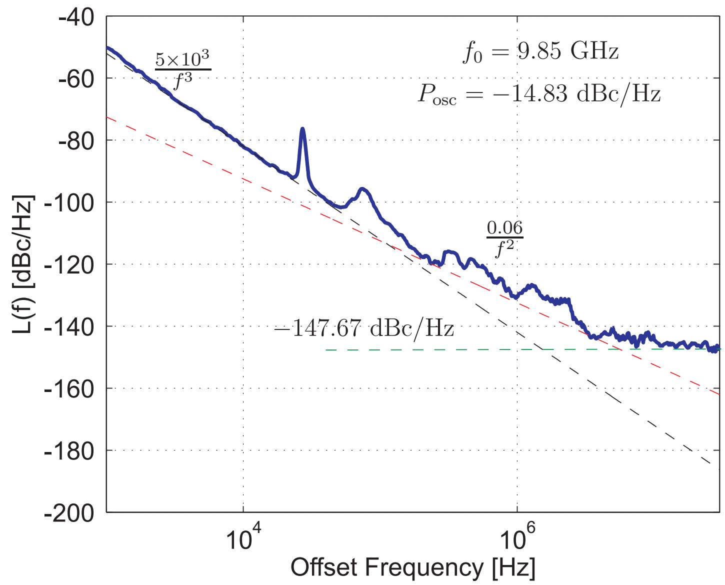

Figure 12: SSB PN spectrum from a GaN HEMT MMIC oscillator. Drain voltage Vdd = 6 V and drain current Id = 30 mA. The corner frequency at f_{corner} = 83.3 kHz.

first, a partial-fraction decomposition of $1/(f^3+\gamma^3)$ is done:

$$\frac{1}{f^3+\gamma^3} = \frac{A}{f-(-\gamma)} + \frac{B}{f-\gamma e^{j\pi/3}} + \frac{C}{f-\gamma e^{-j\pi/3}},$$
$$A = \frac{1}{3\gamma^2},\ B = \frac{e^{-j2\pi/3}}{3\gamma^2},\ C = \frac{e^{j2\pi/3}}{3\gamma^2}. \tag{49}$$

Note that, γ is a real positive number. Using Mathematica (Version 7.0), the following integral can be evaluated

$$\int_0^{+\infty} \frac{1}{f+\beta}\cos(2\pi f\tau)\mathrm{d}f =$$
$$-\cos(2\beta\pi\tau)\mathrm{cosint}(-2\beta\pi|\tau|) - \frac{1}{2}\sin(2\beta\pi|\tau|)(\pi + 2\ \mathrm{sinint}(2\beta\pi|\tau|)), \tag{50}$$

where β must be a complex or a negative real number, and sinint$(\cdot)$ and cosint$(\cdot)$ are sine and cosine integrals define as

$$\mathrm{sinint}(x) = \int_0^{x} \frac{\sin(t)}{t}\mathrm{d}t,$$
$$\mathrm{cosint}(x) = \Gamma + \log(x) + \int_0^{x} \frac{\cos(t)-1}{t}\mathrm{d}t, \tag{51}$$

where $\Gamma \approx 0.5772$ is the Euler-Mascheroni's constant.

Consider the case where time lag τ is small. By Taylor expansion of the functions in (50) around zero

$$\sin(x) = x - \frac{x^3}{6} + \ldots \qquad \cos(x) = 1 - \frac{x^2}{2} + \ldots$$
$$\mathrm{sinint}(x) = x - \frac{x^3}{18} + \ldots \qquad \mathrm{cosint}(x) = \Gamma + \log(x) - \frac{x^2}{4} + \ldots,$$

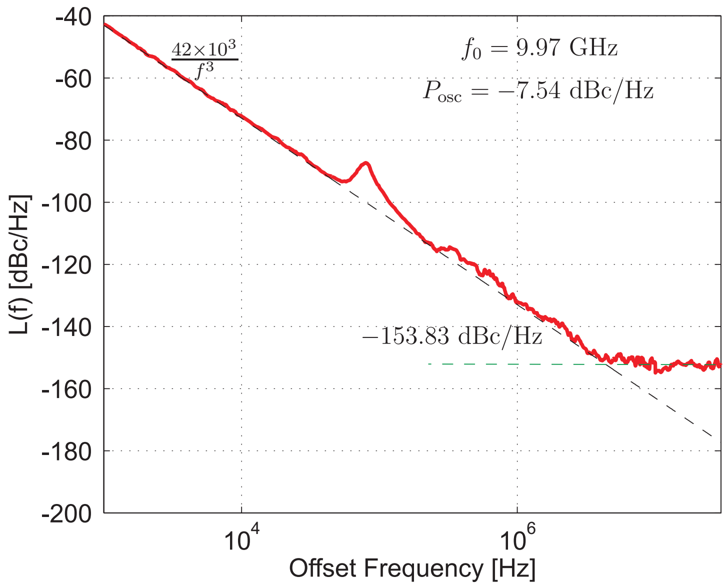

Figure 13: SSB PN spectrum from a GaN HEMT MMIC oscillator. Drain voltage Vdd = 30 V and drain current Id = 180 mA.

and neglecting the terms after second order, the integral can be approximated as

$$\begin{aligned}\int_0^{+\infty} \frac{1}{f+\beta}\cos(2\pi f\tau)\mathrm{d}f \approx \\ &-\Gamma - \log(-2\beta\pi|\tau|) - 2\beta\pi^2|\tau| \\ &+\frac{(2\beta\pi|\tau|)^2}{2}(\Lambda + \log(-2\beta\pi|\tau|)),\end{aligned} \tag{52}$$

where $\Lambda \triangleq \Gamma - \frac{3}{2}$. Employing this approximation and the fraction decomposition in (49), followed by a series of simplifications

$$\int_0^{+\infty} \frac{K_3}{f^3+\gamma^3}\cos(2\pi f\tau)\mathrm{d}f \approx \frac{K_3}{3\gamma^2}\left(\frac{2\pi}{\sqrt{3}} + 6\gamma^2\pi^2\tau^2(\Lambda + \log(2\gamma\pi|\tau|))\right). \tag{53}$$

Now the first term in (48) is calculated. By changing the variable τ to $\tau + T$ and $\tau - T$, second and third terms can also be computed, respectively. Finally, R_{ζ_3} is approximated by

$$\begin{aligned}R_{\zeta_3}(\tau) \approx -8K_3\pi^2\Big[&-\tau^2(\Lambda + \log(2\pi\gamma|\tau|)) \\ &+\frac{(\tau+T)^2}{2}(\Lambda + \log(2\pi\gamma|\tau+T|)) \\ &+\frac{(\tau-T)^2}{2}(\Lambda + \log(2\pi\gamma|\tau-T|))\Big].\end{aligned} \tag{54}$$

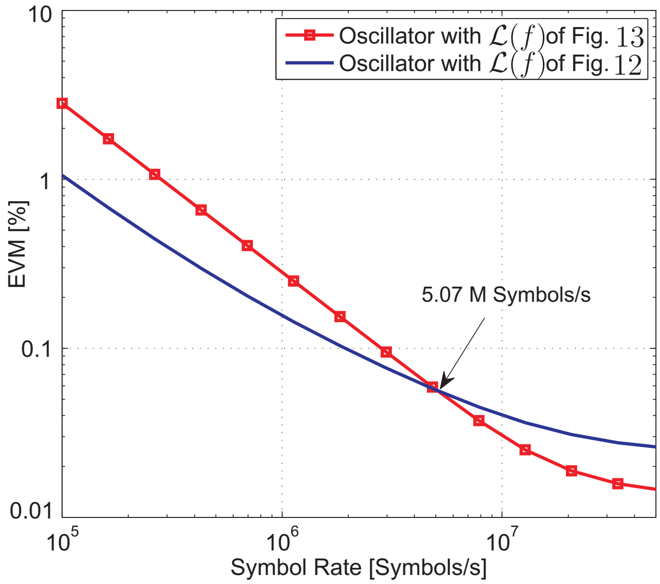

Figure 14: EVM comparison of given measurements in Fig. 12 and 13 vs. symbol rate (bandwidth). The low cut-off frequency γ is considered to be 1 Hz, and SNR=30 dB.

To calculate the ACF for $\tau = 0$, and $\tau = |T|$, we need to take the limits of (54) as τ approaches 0, and $|T|$, respectively that results in

$$\lim_{\tau \to 0} R_{\zeta_3}(\tau) = -8K_3\pi^2T^2(\Lambda + \log(2\pi\gamma T)), \tag{55}$$

$$\lim_{\tau \to |T|} R_{\zeta_3}(\tau) = -8K_3\pi^2T^2(\Lambda + \log(8\pi\gamma T)). \tag{56}$$

References

[1] D. Harris, "Selective demodulation," *Proc. IRE*, vol. 35, no. 6, pp. 565 – 572, Jun. 1947.

[2] A. Viterbi, "Phase-locked loop dynamics in the presence of noise by fokker-planck techniques," *Proc. IEEE*, vol. 51, no. 12, pp. 1737 – 1753, Dec. 1963.

[3] T. Pollet, M. Van Bladel, and M. Moeneclaey, "BER sensitivity of OFDM systems to carrier frequency offset and wiener phase noise," *IEEE Trans. Commun.*, vol. 43, no. 234, pp. 191 –193, Feb./Mar./Apr. 1995.

[4] U. Mengali and M. Morelli, "Data-aided frequency estimation for burst digital transmission," *IEEE Trans. Commun.*, vol. 45, no. 1, pp. 23 –25, Jan. 1997.

[5] H. Meyr, M. Moeneclaey, and S. Fechtel, *Digital Communication Receivers: Synchronization, Channel Estimation, and Signal Processing.* New York, NY, USA: John Wiley & Sons, Inc., 1997.

[6] L. Tomba, "On the effect of wiener phase noise in OFDM systems," *IEEE Trans. Commun.*, vol. 46, no. 5, pp. 580 –583, 1998.

[7] A. Armada and M. Calvo, "Phase noise and sub-carrier spacing effects on the performance of an OFDM communication system," *IEEE Commun. Lett.*, vol. 2, no. 1, pp. 11 –13, 1998.

[8] A. Armada, "Understanding the effects of phase noise in orthogonal frequency division multiplexing (OFDM)," *IEEE Trans. Broadcast.*, vol. 47, no. 2, pp. 153 –159, Jun. 2001.

[9] P. Amblard, J. Brossier, and E. Moisan, "Phase tracking: what do we gain from optimality? particle filtering versus phase-locked loops," *Elsevier Signal Process.*, vol. 83, no. 1, pp. 151 – 167, Mar. 2003.

[10] F. Munier, E. Alpman, T. Eriksson, A. Svensson, and H. Zirath, "Estimation of phase noise for QPSK modulation over AWGN channels," *Proc. GigaHertz 2003 Symp.,* Linköping, Sweden, 2003.

[11] H. Zirath, T. Masuda, R. Kozhuharov, and M. Ferndahl, "Development of 60-ghz front-end circuits for a high-data-rate communication system," *IEEE J. Solid-State Circuits*, vol. 39, no. 10, pp. 1640 – 1649, Oct. 2004.

[12] S. Wu and Y. Bar-Ness, "OFDM systems in the presence of phase noise: consequences and solutions," *IEEE Trans. Commun.*, vol. 52, no. 11, pp. 1988 – 1996, Nov. 2004.

[13] D. Baum and H. Bolcskei, "Impact of phase noise on MIMO channel measurement accuracy," in *Vehicular Tech. Conf. (VTC)*, vol. 3, Sep. 2004, pp. 1614 – 1618.

[14] J. Dauwels and H.-A. Loeliger, "Phase estimation by message passing," *in Proc. IEEE Int. Conf. Commun.*, Jun. 2004.

[15] E. Panayırı, H. Çırpan, and M. Moeneclaey, “A sequential monte carlo method for blind phase noise estimation and data detection,” *in Proc. 13th European Signal Processsing Conf. EUSIPCO*, Sep. 2005.

[16] G. Colavolpe, A. Barbieri, and G. Caire, “Algorithms for iterative decoding in the presence of strong phase noise,” *IEEE J. Sel. Areas Commun.*, vol. 23, pp. 1748–1757, Sep. 2005.

[17] F. Munier, T. Eriksson, and A. Svensson, “An ICI reduction scheme for OFDM system with phase noise over fading channels,” *IEEE Trans. Commun.*, vol. 56, no. 7, pp. 1119 –1126, 2008.

[18] T. Pedersen, X. Yin, and B. Fleury, “Estimation of MIMO channel capacity from phase-noise impaired measurements,” in *IEEE Global Commun. Conf. (GLOBE-COM)*, Dec. 2008, pp. 1 –6.

[19] M. Nissila and S. Pasupathy, “Adaptive iterative detectors for phase-uncertain channels via variational bounding,” *IEEE Trans. Commun.*, vol. 57, no. 3, pp. 716 –725, Mar. 2009.

[20] J. Bhatti and M. Moeneclaey, “Feedforward data-aided phase noise estimation from a DCT basis expansion,” *EURASIP J. Wirel. Commun. Netw.*, Jan. 2009.

[21] M. Dohler, R. Heath, A. Lozano, C. Papadias, and R. Valenzuela, “Is the PHY layer dead?” *IEEE Commun. Mag.*, vol. 49, no. 4, pp. 159 –165, Apr. 2011.

[22] R. Krishnan, H. Mehrpouyan, T. Eriksson, and T. Svensson, “Optimal and approximate methods for detection of uncoded data with carrier phase noise,” in *IEEE Global Commun. Conf. (GLOBECOM)*, Dec. 2011, pp. 1 –6.

[23] R. Krishnan, M.R. Khanzadi, L. Svensson, T. Eriksson, and T. Svensson, “Variational bayesian framework for receiver design in the presence of phase noise in MIMO systems,” in *IEEE Wireless Commun. and Netw. Conf. (WCNC)*, Apr. 2012, pp. 1 –6.

[24] H. Mehrpouyan, A. A. Nasir, S. D. Blostein, T. Eriksson, G. K. Karagiannidis, and T. Svensson, “Joint estimation of channel and oscillator phase noise in MIMO systems,” *IEEE Trans. Signal Process.*, vol. 60, no. 9, pp. 4790 –4807, Sep. 2012.

[25] G. Durisi, A. Tarable, C. Camarda, and G. Montorsi, “On the capacity of MIMO wiener phase-noise channels,” in *Proc. Inf. Theory Applicat. Workshop (ITA)*, Feb. 2013.

[26] R. Krishnan, M.R. Khanzadi, T. Eriksson, and T. Svensson, “Soft metrics and their performance analysis for optimal data detection in the presence of strong oscillator phase noise,” *IEEE Trans. Commun.*, vol. 61, no. 6, pp. 2385 –2395, Jun. 2013.

[27] M. Martalò, C. Tripodi, and R. Raheli, “On the information rate of phase noise-limited communications,” in *Proc. Inf. Theory Applicat. Workshop (ITA)*, Feb. 2013.

[28] H. Ghozlan and G. Kramer, “On wiener phase noise channels at high signal-to-noise ratio,” *arXiv preprint arXiv:1301.6923*, 2013.

[29] ——, "Multi-sample receivers increase information rates for wiener phase noise channels," *arXiv preprint arXiv:1303.6880*, 2013.

[30] S. Bay, C. Herzet, J.-M. Brossier, J.-P. Barbot, and B. Geller, "Analytic and Asymptotic Analysis of Bayesian Cramér Rao Bound for Dynamical Phase Offset Estimation," *IEEE Trans. Signal Process.*, vol. 56, no. 1, pp. 61 –70, Jan. 2008.

[31] Z. Chen and F. Dai, "Effects of LO phase and amplitude imbalances and phase noise on M-QAM transceiver performance," *IEEE Trans. Ind. Electron.*, vol. 57, no. 5, pp. 1505 –1517, May. 2010.

[32] A. Georgiadis, "Gain, phase imbalance, and phase noise effects on error vector magnitude," *IEEE Trans. Veh. Technol.*, vol. 53, no. 2, pp. 443 – 449, Mar. 2004.

[33] A. Demir, "Computing timing jitter from phase noise spectra for oscillators and phase-locked loops with white and $1/f$ noise," *IEEE Trans. Circuits Syst. I, Reg. Papers*, vol. 53, no. 9, pp. 1869 –1884, Sep. 2006.

[34] M.R. Khanzadi, H. Mehrpouyan, E. Alpman, T. Svensson, D. Kuylenstierna, and T. Eriksson, "On models, bounds, and estimation algorithms for time-varying phase noise," in *Int. Conf. Signal Process. Commun. Syst. (ICSPCS)*, Dec. 2011, pp. 1 –8.

[35] A. Demir, "Phase noise and timing jitter in oscillators with colored-noise sources," *IEEE Trans. Circuits Syst. I, Fundam. Theory Appl.*, vol. 49, no. 12, pp. 1782 – 1791, Dec. 2002.

[36] M.R. Khanzadi, A. Panahi, D. Kuylenstierna, and T. Eriksson, "A model-based analysis of phase jitter in RF oscillators," in *IEEE Intl. Frequency Control Symp. (IFCS)*, May 2012, pp. 1 –4.

[37] S. Yousefi and J. Jalden, "On the predictability of phase noise modeled as flicker FM plus white FM," in *Proc. Asilomar Conf.*, Nov. 2010, pp. 1791 –1795.

[38] D. Leeson, "A simple model of feedback oscillator noise spectrum," *Proc. IEEE*, vol. 54, no. 2, pp. 329 – 330, 1966.

[39] J. McNeill, "Jitter in ring oscillators," *IEEE J. Solid-State Circuits*, vol. 32, no. 6, pp. 870 –879, Jun. 1997.

[40] F. Herzel, "An analytical model for the power spectral density of a voltage-controlled oscillator and its analogy to the laser linewidth theory," *IEEE Trans. Circuits Syst. I, Fundam. Theory Appl.*, vol. 45, no. 9, pp. 904 –908, 1998.

[41] A. Hajimiri and T. Lee, "A general theory of phase noise in electrical oscillators," *IEEE J. Solid-State Circuits*, vol. 33, no. 2, pp. 179 –194, 1998.

[42] A. Hajimiri, S. Limotyrakis, and T. Lee, "Jitter and phase noise in ring oscillators," *IEEE J. Solid-State Circuits*, vol. 34, no. 6, pp. 790 –804, Jun. 1999.

[43] G. Klimovitch, "Near-carrier oscillator spectrum due to flicker and white noise," in *Proc. IEEE Intl. Symp. on Circuits Systs.*, vol. 1, Geneva, Switzerland, May 2000, pp. 703 –706 vol.1.

[44] ——, "A nonlinear theory of near-carrier phase noise in free-running oscillators," in *Proc. IEEE Intl. Conf. on Circuits Systs.*, 2000, pp. 1 –6.

[45] A. Demir, A. Mehrotra, and J. Roychowdhury, "Phase noise in oscillators: a unifying theory and numerical methods for characterization," *IEEE Trans. Circuits Syst. I, Fundam. Theory Appl.*, vol. 47, no. 5, pp. 655 –674, May 2000.

[46] C. Liu and J. McNeill, "Jitter in oscillators with $1/f$ noise sources," in *Proc. IEEE 2004 Intl. Symp. on Circuits Systs.*, vol. 1, Vancouver, BC, Canada, May. 2004, pp. 773–776.

[47] A. A. Abidi, "Phase noise and jitter in CMOS ring oscillators," *IEEE J. Solid-State Circuits*, vol. 41, no. 8, pp. 1803–1816, Aug. 2006.

[48] A. Chorti and M. Brookes, "A spectral model for RF oscillators with power-law phase noise," *IEEE Trans. Circuits Syst. I, Reg. Papers*, vol. 53, no. 9, pp. 1989 –1999, 2006.

[49] H. Wang, K.-W. Chang, D.-W. Lo, L. Tran, J. Cowles, T. Block, G. S. Dow, A. Oki, D. Streit, and B. Allen, "A 62-GHz monolithic InP-based HBT VCO," *IEEE Microw. Guided Wave Lett.*, vol. 5, no. 11, pp. 388 –390, Nov. 1995.

[50] S. Gunnarsson, C. Karnfelt, H. Zirath, R. Kozhuharov, D. Kuylenstierna, A. Alping, and C. Fager, "Highly integrated 60 GHz transmitter and receiver MMICs in a GaAs pHEMT technology," *IEEE J. Solid-State Circuits*, vol. 40, no. 11, pp. 2174 – 2186, Nov. 2005.

[51] T. Decker and R. Temple, "Choosing a phase noise measurement technique," in *RF and Microwave Measurement Symposium and Exhibition*, 1999.

[52] J. McNeill, "Jitter in ring oscillators," Ph.D. dissertation, Boston University, 1994.

[53] K. Kundert, "Predicting the phase noise and jitter of PLL-based frequency synthesizers," 2003, [Online]. Available: http://designers-guide.com.

[54] C. Liu, "Jitter in oscillators with $1/f$ noise sources and application to true RNG for cryptography," Ph.D. dissertation, Worcester Polytechnic Institute, 2006.

[55] A. Murat, P. Humblet, and J. Young, "Phase-noise-induced performance limits for DPSK modulation with and without frequency feedback," *J. Lightw. Technol.*, vol. 11, no. 2, pp. 290 –302, Feb. 1993.

[56] J. G. Proakis and M. Salehi,, *Digital communications*, 5th ed. New York: McGraw-Hill, 2008.

[57] R. Hassun, M. Flaherty, R. Matreci, and M. Taylor, "Effective evaluation of link quality using error vector magnitude techniques," in *Proc. Wireless Commun. Conf.*, Aug. 1997, pp. 89 –94.

[58] T. Nakagawa and K. Araki, "Effect of phase noise on RF communication signals," in *Veh. Technol. Conf. (VTC)*, vol. 2, Sep. 2000, pp. 588 –591 vol.2.

[59] S. M. Kay, *Fundamentals of Statistical Signal Processing, Estimation Theory.* Prentice Hall, Signal Processing Series, 1993.

[60] H. L. V. Trees, *Detection, Estimation and Modulation Theory.* New York: Wiley, 1968, vol. 1.

[61] A. D'Andrea, U. Mengali, and R. Reggiannini, "The modified Cramér-Rao bound and its application to synchronization problems," *IEEE Trans. Commun.*, vol. 42, no. 234, pp. 1391 –1399, Feb.-Mar.-Apr. 1994.

[62] R. Corvaja and S. Pupolin, "Effects of phase noise spectral shape on the performance of DPSK systems for wireless applications," *Eur. Trans. Telecommun. (ETT)*, vol. 13, no. 3, pp. 203–210, May. 2002. [Online]. Available: http://dx.doi.org/10.1002/ett.4460130305

[63] J. Havil, *Gamma: exploring Euler's constant.* Princeton, NJ: Princeton University Press, 2003.

[64] N. Kasdin, "Discrete simulation of colored noise and stochastic processes and $1/f$ alpha; power law noise generation," *Proc. IEEE*, vol. 83, no. 5, pp. 802 –827, May 1995.

[65] S. Yousefi, T. Eriksson, and D. Kuylenstierna, "A novel model for simulation of RF oscillator phase noise," in *IEEE Radio and Wireless Symp. (RWS)*, Jan. 2010, pp. 428 –431.

Paper B

Estimation of Phase Noise in Oscillators with Colored Noise Sources

M. Reza Khanzadi, Rajet Krishnan, and Thomas Eriksson

Accepted for publication in
IEEE Communications Letters,
Aug. 2013

Abstract

In this letter we study the design of algorithms for estimation of phase noise (PN) with colored noise sources. A soft-input maximum a posteriori PN estimator and a modified soft-input extended Kalman smoother are proposed. The performance of the proposed algorithms are compared against those studied in the literature, in terms of mean square error of PN estimation, and symbol error rate of the considered communication system. The comparisons show that considerable performance gains can be achieved by designing estimators that employ correct knowledge of the PN statistics.

Keywords: Oscillator Phase Noise, Colored Phase Noise, Maximum a Posteriori Estimator, Extended Kalman Filter/Smoother, Mean Square Error.

1 Introduction

Oscillator phase noise (PN) results in challenging synchronization issues which degrade the performance of communication systems [1, 2]. Demands for high data rates motivate the use of high-order modulation schemes in such systems. Nevertheless, PN severely limits the performance of systems that employ dense constellations.

The problem of PN estimation has been widely studied during the last decades (see [1, 3, 4] and the references therein). In [4], a feedforward PN estimation-symbol detection algorithm is presented, while iterative methods for joint phase estimation and symbol detection are studied in [1].

In prior studies, PN is modeled as a discrete random walk with uncorrelated (white) Gaussian increments between each time instant (i.e., the discrete Wiener process). This model results from using oscillators with white noise sources [5]. However, numerous studies show that real oscillators also contain colored noise sources, and PN is accurately modeled as a random walk with correlated (colored) Gaussian increments [5–7].

In this letter, we propose techniques to estimate PN from real oscillators with white and colored noise sources, in a single antenna-single carrier communication system. We first derive a general soft-input maximum a posteriori (MAP) PN estimator that is optimal in terms of the mean square error (MSE). Then, a modified soft-input extended Kalman smoother is proposed that can be used for estimation of PN with colored increments. The proposed Kalman smoother is observed to perform close to the MAP estimator in several interesting scenarios, with a significantly reduced complexity. Further, we compare the proposed methods with state of the art techniques. The proposed estimators jointly estimate the PN samples of a block of received signals, which improves the estimation performance compared to sequential PN estimation algorithms previously studied (e.g., [3]). Our estimators can be used in feedforward or iterative designs for the estimation of PN with white and colored increments.

2 System Model

Consider the transmission of a block of K data symbols over an additive white Gaussian noise (AWGN) channel, affected by random PN. The channel coefficient from the transmitter to receiver antenna is assumed to be constant over the transmitted block, and it is estimated and compensated by employing a known training sequence that is transmitted prior to the data symbols [2]. In the case of perfect timing synchronization, the received signal after sampling the output of matched filter can be modeled as in [1]

$$y_k = s_k e^{j\theta_k} + w_k,\ \ k \in \{1, \ldots, K\}, \tag{1}$$

where θ_k represents the PN affecting the kth received signal due to noisy transmitter and receiver local oscillators, and w_k is a realization of the independent and identically distributed (i.i.d.) zero-mean complex circularly symmetric AWGN with variance σ^2. In this model, $\mathbf{y} = \{y_k\}_{k=1}^{K}$ is the sequence of received signals and $\mathbf{s} = \{s_k\}_{k=1}^{K}$ is the transmitted symbol sequence divided in two sets of symbols, K_p known pilot symbols, and $K - K_p$ unknown data symbols. We model the pilot and data symbols in general as

$$s_k = \hat{s}_k + \epsilon_k, \tag{2}$$

where $\hat{s}_k$ is the soft detected symbol and ϵ_k models the uncertainty of s_k as an i.i.d zero-mean circularly symmetric AWGN with variance $\sigma^2_{\epsilon_k}$. Such a modeling choice is commonly used in the literature [8]. For the pilot symbols, $\sigma^2_{\epsilon_k} = 0$ since they are known. Using (1) and (2), the received signal can be rewritten as

$$y_k = \hat{s}_k e^{j\theta_k} + \underbrace{\epsilon_k e^{j\theta_k} + w_k}_{\triangleq \tilde{w}_k},\ k \in \{1, \ldots, K\}, \tag{3}$$

where $\tilde{w}_k$ is the new observation noise. As ϵ_k is modeled circularly symmetric, $\tilde{w}_k \sim \mathcal{CN}(0, \sigma_k^2 \triangleq \sigma^2 + \sigma^2_{\epsilon_k})$.

The PN samples are modeled by a random-walk as

$$\theta_k = \theta_{k-1} + \zeta_{k-1}, \tag{4}$$

where the phase increment process ζ_k is a zero-mean Gaussian random process. Recent studies of the PN in oscillators with colored noise sources show that the PN increments can be correlated over time [5–7]. Hence, we consider a general case where the autocorrelation function of ζ_k, denoted as $R_\zeta(l)$, is known a priori. Note that the Wiener PN model extensively used in the literature is a special case of the proposed model, with uncorrelated (white) phase increments [5].

3 Phase Noise Estimation

In the sequel, we propose two methods for joint estimation of K-dimensional PN vector $\boldsymbol{\theta} = \{\theta_k\}_{k=1}^K$, that further would be used for data detection. First, we derive a MAP estimator. Thereafter, we propose an approach for modification of (4), such that smoothing algorithms (e.g., Kalman smoother) with a lower complexity than MAP can be used for estimation.

3.1 Proposed MAP Estimator

Let $f(\boldsymbol{\theta}|\mathbf{y})$ denote the a posteriori distribution of PN vector $\boldsymbol{\theta}$, given the observation vector $\mathbf{y}$. The MAP estimator of $\boldsymbol{\theta}$ is determined as

$$\hat{\boldsymbol{\theta}} = \arg\max_{\boldsymbol{\theta}} \log(f(\boldsymbol{\theta}|\mathbf{y})) = \arg\max_{\boldsymbol{\theta}} \log(f(\mathbf{y}|\boldsymbol{\theta}) f(\boldsymbol{\theta})), \tag{5}$$

where we define $\ell(\boldsymbol{\theta}) \triangleq \log(f(\mathbf{y}|\boldsymbol{\theta}) f(\boldsymbol{\theta}))$. To solve this optimization, we first need to find the likelihood, $f(\mathbf{y}|\boldsymbol{\theta})$, and prior distribution of $\boldsymbol{\theta}$, $f(\boldsymbol{\theta})$. As both w_k and ϵ_k are i.i.d, and y_k only depends on θ_k according to (3), the likelihood function can be written as

$$f(\mathbf{y}|\boldsymbol{\theta}) = \prod_{k=1}^{K} f(y_k|\boldsymbol{\theta}) = \prod_{k=1}^{K} f(y_k|\theta_k), \tag{6}$$

Notations: Italic letters (x) are scalar variables, boldface letters ($\mathbf{x}$) are vectors, uppercase boldface letters ($\mathbf{X}$) are matrices, ($[\mathbf{X}]_{a,b}$) denotes the $(a, b)^{th}$ entry of matrix $\mathbf{X}$, diag($\mathbf{X}$) denotes the diagonal elements of matrix ($\mathbf{X}$), $\mathbb{E}[\cdot]$ denotes the statistical expectation operation, $\mathcal{CN}(x; \mu, \sigma^2)$ denotes the complex proper Gaussian distribution function, where x is the variable, μ is the mean and σ^2 is the variance, $\log(\cdot)$ denotes the natural logarithm, $\Re\{\cdot\}$, $\Im\{\cdot\}$, and $\arg\{\cdot\}$ are the real part, imaginary part, and angle of complex-valued numbers, and $(\cdot)^*$ and $(\cdot)^T$ denote the conjugate and transpose, respectively.

where

$$f(y_k|\theta_k) = \mathcal{CN}(y_k; \hat{s}_k e^{j\theta_k}, \sigma_k^2) = \frac{1}{\sigma_k^2 \pi} \exp\left(-\frac{|y_k - \hat{s}_k e^{j\theta_k}|^2}{\sigma_k^2}\right). \tag{7}$$

In order to find the prior distribution $f(\boldsymbol{\theta})$ of the PN vector, we use the random walk model in (4) that results in a general PN incremental form of

$$\theta_k = \theta_1 + \sum_{i=1}^{k-1} \zeta_i, \tag{8}$$

where θ_1 (PN of the first symbol in the block) is modeled as a zero-mean Gaussian random variable with a high variance[1], denoted as $\sigma_{\theta_1}^2$. Based on (8), we can show that $\boldsymbol{\theta}$ has a multivariate Gaussian distribution $f(\boldsymbol{\theta}) = \mathcal{N}(\boldsymbol{\theta}; \mathbf{0}, \mathbf{C})$ where elements of the covariance matrix $\mathbf{C}$ can be computed as

$$\begin{aligned}[\mathbf{C}]_{m,m'} &= \mathbb{E}\Big[(\theta_m - \mathbb{E}[\theta_m])(\theta_{m'} - \mathbb{E}[\theta_{m'}])\Big] \\ &= \sigma_{\theta_1}^2 + \sum_{l=1}^{m-1}\sum_{l'=1}^{m'-1} R_\zeta(l-l'), \quad m, m' \in \{1, \ldots, K\}.\end{aligned} \tag{9}$$

From (7) and the multivariate Gaussian prior of $\boldsymbol{\theta}$ we obtain

$$\ell(\boldsymbol{\theta}) = \sum_{k=1}^{K} \frac{2}{\sigma_k^2} \Re\{y_k \hat{s}_k^* e^{-j\theta_k}\} - \frac{1}{2}(\boldsymbol{\theta}^T \mathbf{C}^{-1} \boldsymbol{\theta}) + const. \tag{10}$$

To find the maximizer of (10), an exhaustive grid-search over all possible values of $\boldsymbol{\theta}$ can be used. However, the complexity of this method increases exponentially with the length of $\boldsymbol{\theta}$. The stationary point of this optimization can analytically be found as the root of the gradient of $\ell(\boldsymbol{\theta})$ with respect to $\boldsymbol{\theta}$,

$$\mathbf{g}(\boldsymbol{\theta}) \triangleq 2\left[\left\{\frac{\Im\{y_k \hat{s}_k^* e^{-j\theta_k}\}}{\sigma_k^2}\right\}_{k=1}^{K}\right]^T - \mathbf{C}^{-1}\boldsymbol{\theta} = \mathbf{0}. \tag{11}$$

In order to solve $\mathbf{g}(\boldsymbol{\theta}) = \mathbf{0}$, which is a non-linear system of equations, we use the Newton–Raphson method whose nth iteration is given by

$$\hat{\boldsymbol{\theta}}^{(n+1)} = \hat{\boldsymbol{\theta}}^{(n)} - \mathbf{H}^{-1}(\hat{\boldsymbol{\theta}}^{(n)})\mathbf{g}(\hat{\boldsymbol{\theta}}^{(n)}), \tag{12}$$

where $\mathbf{H}(\boldsymbol{\theta})$ denotes the Hessian matrix,

$$\mathbf{H}(\boldsymbol{\theta}) \triangleq -\left(2\,\mathrm{diag}\left(\left[\left\{\frac{\Re\{y_k \hat{s}_k^* e^{-j\theta_k}\}}{\sigma_k^2}\right\}_{k=1}^{K}\right]\right) + \mathbf{C}^{-1}\right). \tag{13}$$

We iterate till an accurate value of the root is reached.

[1]We consider a flat non-informative prior [9] for the initial PN value, modeled by a Gaussian distribution with a high variance that behaves similar to a flat prior over a certain interval.

To show that this algorithm reaches a global maximum, we first prove that $\ell(\boldsymbol{\theta})$ is a concave function in moderate and high signal to noise ratio (SNR) regimes. In (13), $\mathbf{C}^{-1}$ is the inverse of a covariance matrix, thus it is a positive-definite matrix. If the first term of the sum in (13) is also positive-definite (or positive-semidefinite), the Hessian becomes negative-definite, thus implying that $\ell(\boldsymbol{\theta})$ is a concave function. For the first term of (13) to be positive-semidefinite, $\Re\{y_k \hat{s}_k^* e^{-j\theta_k}\}$ must be greater than or equal to zero. Exploiting Eq. (3) we get

$$\Re\{y_k \hat{s}_k^* e^{-j\theta_k}\} = |\hat{s}_k|^2 + \Re\{\hat{s}_k^* \breve{w}_k\} \geq 0, \tag{14}$$

where $\breve{w}_k \triangleq e^{-j\theta_k}\tilde{w}_k$ with the same statistics as $\tilde{w}_k$. It is clear that for moderate and high SNR, (14) is satisfied with a high probability, and consequently $\ell(\boldsymbol{\theta})$ is a concave function.

In the low-SNR regime, $\ell(\boldsymbol{\theta})$ is not necessarily concave. Therefore, we propose an approach to initiate the iterations with a guess which is fairly close to the optimal point. This ensures that the method does not get trapped in a local maxima, far from the global maximum. Moreover, employing a good initial guess speeds up the convergence of the algorithm at any SNR. In this respect, we first find the maximum likelihood (ML) estimate of the PN samples for the pilot symbols. For any s_k in the pilot set, the ML estimator of the kth PN sample can be computed as $\hat{\theta}_k^{\mathrm{ML}} = \arg\{y_k s_k^*\}$. Then, we form our initial estimate of the PN vector, $\hat{\boldsymbol{\theta}}^{(0)}$, as the linear interpolation of the ML estimated PN values.

The MAP estimator is an optimal minimum mean square estimator if its MSE attains the Bayesian Cramér-Rao bound (BCRB) [9]. In the Appendix, we analytically derive the MSE of the MAP, and show that it is approximately equal to the BCRB of the PN estimation. Our simulation results in Sec. IV also confirms this (Fig. 2).

Although, the proposed MAP estimator gives an optimal estimate of $\boldsymbol{\theta}$, as we can see in (12), it involves inversion of $K \times K$ matrices that may raise some complexity issues. In the next section, we propose an approach to modify the PN model and reduce the complexity.

3.2 Auto Regressive Model of Colored Phase Noise Increments

In general, the PN increment process can be modeled with a pth-order auto regressive (AR) process as follows

$$\zeta_k = \sum_{i=1}^{p} \alpha_i \zeta_{k-i} + \Delta_k, \tag{15}$$

where α_i are the coefficients of the AR model and Δ_k is modeled as a zero-mean white noise process with variance σ_Δ^2. For a given autocorrelation $R_\zeta(l)$ and AR order p, the optimal α_i and σ_Δ^2 can be computed using algorithms such as the Levinson-Durbin recursion. We modify the state equation (4) with the AR model (15), which results in an augmented state equation,

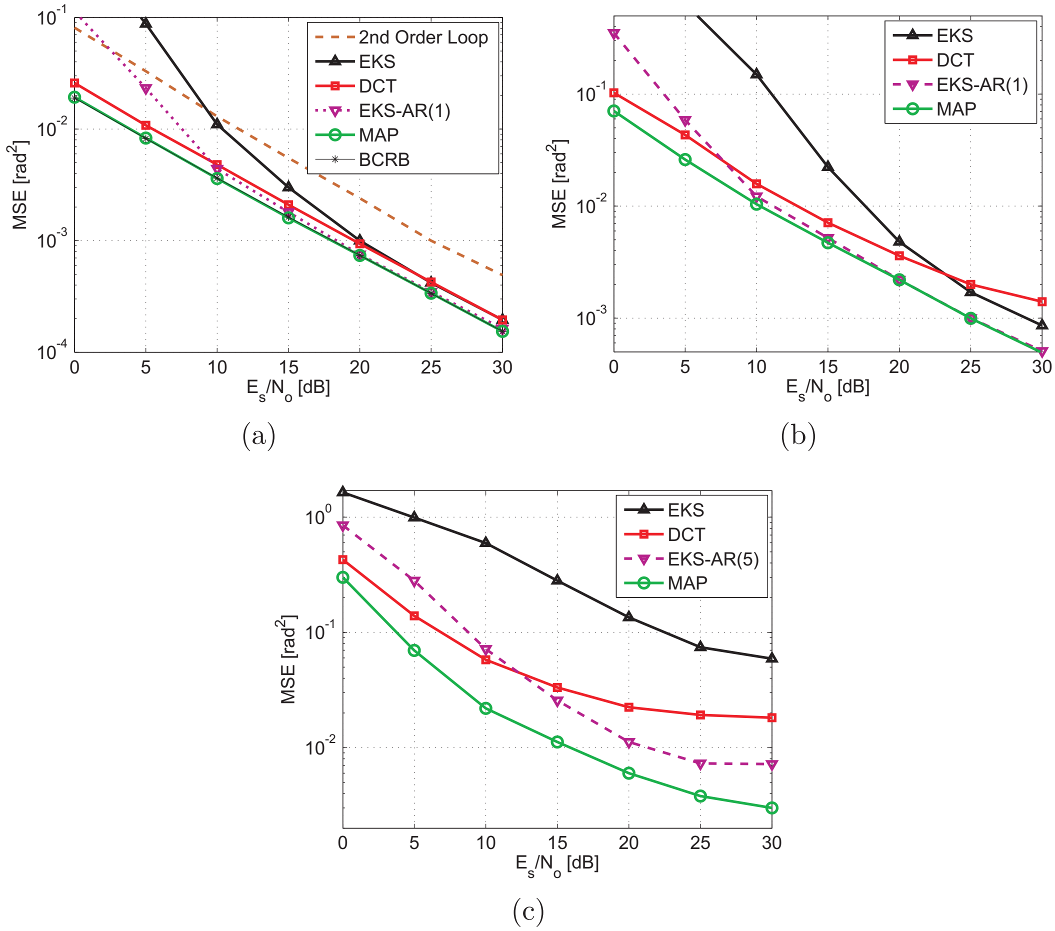

Figure 1: MSE comparison of different PN estimation methods for different pilot densities over a block of $K = 101$ symbols. Phase increment is colored with variance $R_\zeta(0) = 10^{-3}[\text{rad}^2]$. (a) Data-aided case, where all symbols are pilots. (b) Pilot density of 21%. (c) Pilot density of 6%.

$$\underbrace{\begin{bmatrix} \theta_k \\ \zeta_k \\ \zeta_{k-1} \\ \vdots \\ \zeta_{k-p} \end{bmatrix}}_{\triangleq \mathbf{x}_k} = \underbrace{\begin{bmatrix} 1 & 1 & 0 & \dots & 0 \\ 0 & \alpha_1 & \alpha_2 & \dots & \alpha_p \\ 0 & 1 & 0 & \dots & 0 \\ \vdots & \ddots & \ddots & \ddots & \vdots \\ 0 & \dots & 0 & 1 & 0 \end{bmatrix}}_{\triangleq \mathbf{F}} \underbrace{\begin{bmatrix} \theta_{k-1} \\ \zeta_{k-1} \\ \zeta_{k-2} \\ \vdots \\ \zeta_{k-p-1} \end{bmatrix}}_{\triangleq \mathbf{x}_{k-1}} + \underbrace{\begin{bmatrix} 0 \\ \Delta_k \\ 0 \\ \vdots \\ 0 \end{bmatrix}}_{\triangleq \boldsymbol{\Delta_{k-1}}}, \tag{16}$$

where $\mathbf{x}_k$ is the new state vector that has a higher dimension compared to our original state variable θ_k, and $\boldsymbol{\Delta_k}$ denotes the new process noise that is white, with covariance

$$\mathbb{E}[\boldsymbol{\Delta}_k \boldsymbol{\Delta}_k^T] = \text{diag}\left([0, \sigma_\Delta^2, 0, \dots, 0]\right). \tag{17}$$

We can use the new state equation (16) along with the observation model (3) to estimate $\boldsymbol{\theta}$ by Kalman filtering/smoothing [9]. For the colored PN increments with a long memory, normally a high-order AR model is needed that results in a high dimensional state equation (16). In order to reduce complexity, we approximate the colored PN increments with a low-order AR process. Numerical simulations in Sec. 4 show that even with such an approximation, the modified extended Kalman smoother (EKS) perform close to the proposed MAP estimator, in several scenarios of interest.

4 Numerical Results

We now study the performance of our proposed estimators and compare with that of those available in the literature (e.g., [1, 3, 4]). We consider transmission of a block of $K = 101$ 16-QAM modulated symbols, with uniformly distributed pilots. For simulation of the PN with colored noise increments, we use the results of [6, 7], where the autocorrelation function of the PN increments for oscillators with a colored noise source (flicker noise) has been derived. We set the parameters such that the variance of the PN increments becomes $R_\zeta(l = 0) = 10^{-3}[\text{rad}^2]$.

It can be seen in Fig. 1-(a) that the MSE of the proposed MAP estimator reaches the BCRB [7] in the data-aided case, where all symbols are pilots. We stop the optimization algorithm when the gradient is sufficiently small (here $|\mathbf{g}(\boldsymbol{\theta})| < 10^{-6}$). We observe that the number of required iterations for satisfying any level of accuracy depends on various parameters such as the block length, the PN statistics, the pilot density and the SNR. In general, for most practical scenarios less that 5 iterations suffice. For instance, for simulations of Fig. 1 with 6% pilot density, at SNRs 0 and 30 dB, on average 4.3 and 2.95 iterations are required, respectively.

The MSE of the PN estimator proposed in [4], based on interpolation of the PN estimates of the pilot symbols using discrete cosine transform (DCT), is close to the MAP estimator in the data-aided case. However, decreasing the pilot density in Fig. 1-(b) and (c) to 21% and 6%, shows that the DCT-based estimator performs poorly in low-pilot density scenarios. The reason is that this estimator is blind to the statistics of the PN process that limits its performance when the received signals are not reliable.

Using an EKS designed for white PN increments in the colored case results in large MSEs in low-SNR and low-pilot density cases. In high-pilot density scenarios, the observations are reliable and the EKS performs close to the MAP. When the pilot density is low, the tested EKS relies on PN statistics that are not matched to the real process, which results in large MSEs. Now consider the modified EKS designed with the low-order AR approximation. Using a first-order AR model, the modified EKS reaches the MSE of the MAP in the data-aided and 21% pilot density cases. With 6% pilot density, where the modified EKS relies more on the PN statistics, a higher order AR model is needed to improve the performance ($p > 5$). Fig. 1-(a) also shows the data-aided MSE of the second-order phase tracking loop [3].

Fig. 2 shows that the simulated MSE of the MAP estimator reaches the BCRB. Fig. 3 and 4 compare the effect of using the discussed estimators on symbol error rate (SER) of the system, after three iterations between the PN estimators and a Euclidian-distance-based symbol detector. Mean and variance of the soft symbols are calculated as the mean and variance of the symbols' a posteriori probabilities. In both scenarios, the MAP esti-

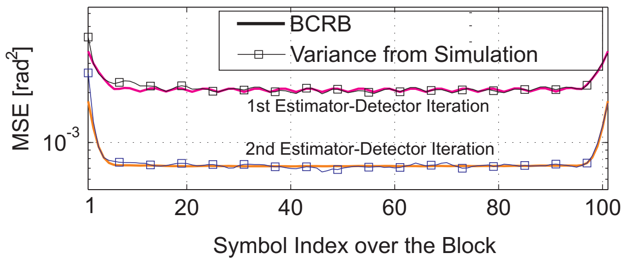

Figure 2: Simulated variance of MAP vs. BCRB. Pilot density 21%, $R_\zeta(0) = 10^{-3}[\text{rad}^2]$, SNR $= 20$[dB].

mator outperforms other estimators. It can also be seen that in the 6% density compared to 21% scenario, a higher order AR model is needed for more accurate approximation of the colored PN increments. In addition to the estimators in Fig. 1, we also study the performance of an iterative receiver that is designed based on the sum-product algorithm (SPA) [1]. This SPA-based receiver performs extremely well in presence of the Wiener PN, but it is not designed for PN with colored increments.

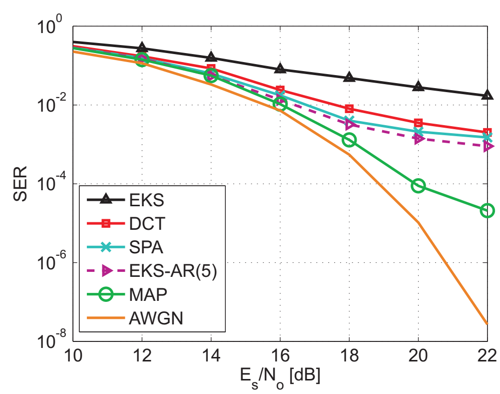

Figure 3: SER comparison of different PN estimation methods after three estimation-detection iterations. Pilot density 6% and $R_\zeta(0) = 10^{-3}[\text{rad}^2]$.

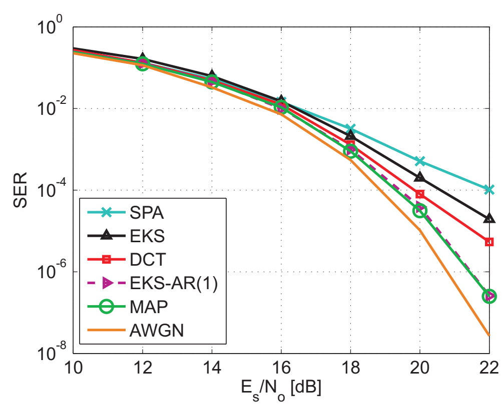

Figure 4: SER comparison of different PN estimation methods after three estimation-detection iterations. Pilot density 21% and $R_\zeta(0) = 10^{-3}[\text{rad}^2]$.

5 Conclusions

In this letter, we showed that deriving the soft-input maximum a posteriori (MAP) estimator for estimation of phase noise (PN) in oscillators with colored noise sources is a concave optimization problem at moderate and high SNRs. Further, we showed that the modified soft-input extended Kalman smoother with low-order AR approximation of the colored PN increments performs close to the MAP in several scenarios. From simulations, we observed that considerable performance gain can be achieved by using the proposed estimators compared to estimators that lack correct statistic of the PN. The gain is more significant in low-SNR or low-pilot density scenarios.

6 Appendix

Here, we find the mean and covariance of the MAP estimation error, defined as $\boldsymbol{\psi} \triangleq (\boldsymbol{\theta}^\dagger - \hat{\boldsymbol{\theta}})$, where $\boldsymbol{\theta}^\dagger$ denotes the true value of $\boldsymbol{\theta}$. We first write the Taylor expansion of $\mathbf{g}(\boldsymbol{\theta})$ around $\boldsymbol{\theta}^\dagger$ and evaluate it at $\hat{\boldsymbol{\theta}}$. Assuming that $\hat{\boldsymbol{\theta}}$ is close to $\boldsymbol{\theta}^\dagger$, we can neglect the higher order terms and obtain

$$\mathbf{g}(\hat{\boldsymbol{\theta}}) \approx \mathbf{g}(\boldsymbol{\theta}^\dagger) + \mathbf{H}(\boldsymbol{\theta}^\dagger)(\hat{\boldsymbol{\theta}} - \boldsymbol{\theta}^\dagger). \tag{18}$$

Note that $\hat{\boldsymbol{\theta}}$ is the root of $\mathbf{g}(\boldsymbol{\theta}) = \mathbf{0}$. Therefore,

$$\boldsymbol{\theta}^\dagger = \hat{\boldsymbol{\theta}} + \mathbf{H}^{-1}(\boldsymbol{\theta}^\dagger)\mathbf{g}(\boldsymbol{\theta}^\dagger), \tag{19}$$

where $\boldsymbol{\psi} \triangleq (\boldsymbol{\theta}^\dagger - \hat{\boldsymbol{\theta}}) = \mathbf{H}^{-1}(\boldsymbol{\theta}^\dagger)\mathbf{g}(\boldsymbol{\theta}^\dagger)$ is the estimation error term whose mean is calculated as

$$\mathbb{E}[\boldsymbol{\psi}] = \mathbb{E}[\mathbf{H}^{-1}(\boldsymbol{\theta}^\dagger)\mathbf{g}(\boldsymbol{\theta}^\dagger)]. \tag{20}$$

Setting the value of y_k from (3) in (11) and (13) gives

$$\mathbf{g}(\boldsymbol{\theta}^\dagger) = 2\left[\left\{\frac{\Im\{\hat{s}_k^* \check{w}_k\}}{\sigma_k^2}\right\}_{k=1}^{K}\right]^T - \mathbf{C}^{-1}\boldsymbol{\theta}^\dagger, \tag{21a}$$

$$\mathbf{H}(\boldsymbol{\theta}^\dagger) = -2\,\mathrm{diag}\left(\left[\left\{\frac{|\hat{s}_k|^2 + \Re\{\hat{s}_k^* \check{w}_k\}}{\sigma_k^2}\right\}_{k=1}^{K}\right]\right) - \mathbf{C}^{-1}, \tag{21b}$$

where $\check{w}_k \triangleq e^{-j\theta_k}\tilde{w}_k$ with the same statistics as $\tilde{w}_k$. It is clear that $\mathbf{H}(\boldsymbol{\theta}^\dagger)$ and $\mathbf{g}(\boldsymbol{\theta}^\dagger)$ are independent. Therefore,

$$\mathbb{E}[\boldsymbol{\psi}] = \mathbb{E}[\mathbf{H}^{-1}(\boldsymbol{\theta}^\dagger)]\mathbb{E}[\mathbf{g}(\boldsymbol{\theta}^\dagger)] = \mathbf{0}, \tag{22}$$

where the second equality is true because $\mathbb{E}[\mathbf{g}(\boldsymbol{\theta}^\dagger)] = \mathbf{0}$.

The covariance matrix of $\boldsymbol{\psi}$ is determined as

$$\boldsymbol{\Sigma} = \mathbb{E}[\boldsymbol{\psi}\boldsymbol{\psi}^T] = \mathbb{E}[\mathbf{H}^{-1}(\boldsymbol{\theta}^\dagger)\mathbf{g}(\boldsymbol{\theta}^\dagger)\mathbf{g}^T(\boldsymbol{\theta}^\dagger)\mathbf{H}^{-1}(\boldsymbol{\theta}^\dagger)]. \tag{23}$$

In (21b), it is possible to neglect $\Re\{\hat{s}_k^* \tilde{w}_k\}$ compared to $|\hat{s}_k|^2$ for moderate and high SNRs. Therefore, $\mathbf{H}(\boldsymbol{\theta}^\dagger)$ is approximated as

$$\mathbf{H}(\boldsymbol{\theta}^\dagger) \approx \tilde{\mathbf{H}}(\boldsymbol{\theta}^\dagger) = -2\,\mathrm{diag}\left(\left[\left\{\frac{|\hat{s}_k|^2}{\sigma_k^2}\right\}_{k=1}^{K}\right]\right) - \mathbf{C}^{-1}, \tag{24}$$

which is a deterministic matrix. Thus, the expectation in (23) is only over $\mathbf{g}(\boldsymbol{\theta}^\dagger)\mathbf{g}^T(\boldsymbol{\theta}^\dagger)$.

Based on (21a) and after straightforward mathematical manipulation,

$$\mathbb{E}[\mathbf{g}(\boldsymbol{\theta}^\dagger)\mathbf{g}^T(\boldsymbol{\theta}^\dagger)] = -\tilde{\mathbf{H}}(\boldsymbol{\theta}^\dagger), \tag{25}$$

and hence, $\boldsymbol{\Sigma} \approx -\tilde{\mathbf{H}}^{-1}(\boldsymbol{\theta}^\dagger)$. Employing the data-aided BCRB for estimation of colored PN derived in [7], and using the system model (3), it is straightforward to find the soft-input BCRB, and show that it is identical to the covariance of estimation error $\boldsymbol{\Sigma}$.

References

[1] G. Colavolpe, A. Barbieri, and G. Caire, "Algorithms for iterative decoding in the presence of strong phase noise," *IEEE J. Sel. Areas Commun.*, vol. 23, pp. 1748–1757, Sep. 2005.

[2] H. Mehrpouyan, A. A. Nasir, S. D. Blostein, T. Eriksson, G. K. Karagiannidis, and T. Svensson, "Joint estimation of channel and oscillator phase noise in MIMO systems," *IEEE Trans. Signal Process.*, vol. 60, no. 9, pp. 4790 –4807, Sep. 2012.

[3] P. Amblard, J. Brossier, and E. Moisan, "Phase tracking: what do we gain from optimality? particle filtering versus phase-locked loops," *Elsevier Signal Process.*, vol. 83, no. 1, pp. 151 – 167, Mar. 2003.

[4] J. Bhatti and M. Moeneclaey, "Feedforward data-aided phase noise estimation from a DCT basis expansion," *EURASIP J. Wirel. Commun. Netw.*, Jan. 2009.

[5] A. Demir, "Computing timing jitter from phase noise spectra for oscillators and phase-locked loops with white and $1/f$ noise," *IEEE Trans. Circuits Syst. I, Reg. Papers*, vol. 53, no. 9, pp. 1869 –1884, Sep. 2006.

[6] M.R. Khanzadi, A. Panahi, D. Kuylenstierna, and T. Eriksson, "A model-based analysis of phase jitter in RF oscillators," in *IEEE Intl. Frequency Control Symp. (IFCS)*, May 2012, pp. 1 –4.

[7] M.R. Khanzadi, D. Kuylenstierna, T. Eriksson, and H. Zirath, "Calculation of the performance of communication systems from measured oscillator phase noise," *Submitted to IEEE Trans. Circuits Syst. I, Reg. Papers*, [Online]. Available: http://arxiv.org/abs/1305.1187.

[8] S. Song, A. C. Singer, and K. M. Sung, "Soft input channel estimation for turbo equalization," *IEEE Trans. Signal Process.*, vol. 52, no. 10, pp. 2885–2894, Oct. 2004.

[9] S. M. Kay, *Fundamentals of Statistical Signal Processing, Estimation Theory.* Prentice Hall, Signal Processing Series, 1993.